CDK5RAP2 REGULATES CENTRIOLE LICENSING TO RESTRICT CENTRIOLE DUPLICATION IN MICE

APPROVED BY SUPERVISORY COMMITTEE

Timothy L. Megraw, Ph.D.

Robert E. Hammer, Ph.D.

William J. Snell, Ph.D.

Hui Zou, Ph.D.

DEDICATION

I dedicate my thesis to my family for their love, encouragement and sacrifices. I especially thank my lovely wife, Lisa M. Barrera, for her unwavering love, support and understanding. Without her none of this would have been possible.

# CDK5RAP2 REGULATES CENTRIOLE LICENSING TO RESTRICT CENTRIOLE DUPLICATION IN MICE

by

JOSE ANSELMO BARRERA

DISSERTATION / THESIS

Presented to the Faculty of the Graduate School of Biomedical Sciences

The University of Texas Southwestern Medical Center at Dallas

In Partial Fulfillment of the Requirements

For the Degree of

DOCTOR OF PHILOSOPHY

The University of Texas Southwestern Medical Center at Dallas

Dallas, Texas

June, 2009

CDK5RAP2 REGULATES CENTRIOLE LICENSING TO RESTRICT CENTRIOLE DUPLICATION IN MICE

JOSE ANSELMO BARRERA, Ph.D.

The University of Texas Southwestern Medical Center at Dallas, 2009

TIMOTHY LEXOW MEGRAW, Ph.D.

Cells division is a highly coordinated series of events that must occur with extreme precision. Defects during segregation of genetic material (DNA) can have adverse effects on the health of the cell, surrounding tissue, organ, and the organism as a whole. Accurate assembly of the bipolar mitotic spindle apparatus is crucial for precise chromosome segregation. Centrosomes play a crucial role in establishment of the mitotic spindle and therefore are vital to the maintenance of genetic stability. Centrosomes are composed of two centrioles that arrange a specialized conglomerate of proteins into a pericentriolar matrix. Centrosomes are highly regulated throughout the cell cycle, and

duplicate only once per cell cycle ensuring that each cell inherits one centrosome after mitotic exit, and contains only two centrosomes at the following mitosis.

Truncating mutations in the *Cyclin-Dependent Kinase 5 Regulatory Associated Protein 2* gene (*CDK5RAP2*), which encodes a centrosomal protein, result in autosomal recessive primary microcephaly (MCPH, [MIM 251200]) in humans. The major phenotypic manifestation of this rare genetic disorder is a small head. Affected individuals have head circumferences at least 4 standard deviations below sex- and age-matched individuals and suffer mental retardation.

In order to investigate how mutations in *CDK5RAP2* affect centrosome structure and regulation, and how this leads to MCPH, we derived two distinct mouse mutant lines with truncating mutations within the *CDK5RAP2* locus similar to those found in affected humans. We show that centriole engagement and cohesion, two distinct centriole-binding processes, are disrupted in *CDK5RAP2* mutant cells. Partial disruption of *CDK5RAP2* affected centriole cohesion, whereas complete *CDK5RAP2* disruption deregulated the centriole duplication cycle leading to centriole/centrosome amplification. During mitosis amplified centrosomes in *CDK5RAP2* mutant cells were potent microtubule organizing centers that drove formation of multipolar spindles. Furthermore, cells formed multiple primary cilia from multiple centrioles inherited from the previous cell cycle. Together these results define a role for CDK5RAP2 in the regulation of centriole duplication and also provide a basis for the development of MCPH.

TABLE OF CONTENTS

## PRIOR PUBLICATIONS

Huang, J., Wu, S., Barrera, J., Matthews, K., and Pan, D. (2005). The Hippo signaling pathway coordinately regulates cell proliferation and apoptosis by inactivating Yorkie, the Drosophila Homolog of YAP. Cell 122, 421-434.

LIST OF FIGURES

LIST OF TABLES

LIST OF DEFINITIONS

CDK5RAP2 – Cyclin-Dependent Kinase 5 Regulatory Associated Protein 2

*C. elegans – Caenorhabditis elegans*

CNN – Centrosomin

DAPI – 4',6-diamidino-2-phenylindole

DIC – differential interference contrast

DNA – deoxyribonucleic acid

GFP – green fluorescent protein

H&E – hematoxylin and eosin

MCPH – Autosomal Recessive Primary Microcephaly

MEFs – mouse embryonic fibroblasts

MTOC – microtubule organizing center

ODF2 – outer dense fiber 2

NEBD – nuclear envelope breakdown

PCM – pericentriolar matrix

PI – propidium iodine

# CHAPTER ONE

# INTRODUCTION

## A. Centrosome

### *Overview*

Theodor Boveri, a German biologist, first described the centrosome in 1888. Since that discovery, the centrosome has been recognized as a key organelle in cell division. Boveri observed that amplified centrosomes could induce unfaithful segregation of DNA and hypothesized that amplified centrosomes could lead to the development of cancer (Potter, 2008). Centrosomes are the major microtubule organizing centers (MTOC) within most animal cells. Performing distinct functions during different stages of the cell cycle. Chief among them are their involvement in formation of cilia and flagella, the interphase microtubule network, the mitotic spindle, and cell polarization.

### *Centrosome Structure*

The centrosome is a non-membranous organelle composed of a pair of centrioles that assemble a set of proteins into an amorphous pericentriolar matrix (PCM), a proteinaceous material that supports microtubule nucleation, polymerization, and stabilization (Doxsey, 2001; Bornens, 2002; Luders and Stearns, 2007). A centriole pair consist of an older mature “mother” centriole and an immature “daughter” centriole, that are structurally and functionally distinct (Vorobjev and Chentsov Yu, 1982; Paintrand et al., 1992). Unlike centrioles, which are highly stable upon formation, the PCM is an

extremely dynamic region of the centrosome that involves the recruitment of structural proteins, kinases, and phosphatases that display temporal regulation during the cell cycle.

*Centriole Structure*

Centrioles are barrel shaped structures composed of triplet microtubule blades organized into an elegant 9-fold symmetrical cylinder (Bettencourt-Dias and Glover, 2007; Strnad and Gonczy, 2008). Centriole duplication is a template driven process and newborn daughters assemble from the base of pre-existing centrioles, resulting in the quintessential orthogonal centriole arrangement. Mother centrioles are distinguished by distal and sub-distal appendages, added one and one-half cell cycles after their formation, that are absent in daughter centrioles (Vorobjev and Chentsov Yu, 1982; Paintrand et al., 1992). Early in G1-phase, the mother centriole serves as the basal body for the primary cilium, a function dependent on distal and sub-distal appendages. In the absence of centrioles, PCM becomes unstable, dispersed, and is unable to support microtubule nucleation (Bobinnec et al., 1998). Although prototypical centrosomes consist of centriole pairs, a single centriole can also assemble functional PCM. Therefore, centrosome numbers are determined not only by regulation of centriole duplication but also by the number of single and paired centrioles.

Recent molecular genetic epistasis relationships have defined a signaling pathway for centriole formation in *Caenorhabditis elegans (C. elegans)*. Proteins involved in this pathway are listed in the order of their function: Spd-2, Zyg-1, Sas5, Sas6, and Sas4 (O'Connell et al., 2001; Kirkham et al., 2003; Leidel and Gonczy, 2003; Delattre et al., 2004; Kemp et al., 2004; Pelletier et al., 2004; Leidel et al., 2005). Spd-2

and Zyg-1 are the upstream signals that initiate centriole assembly. Subsequently, Sas5 and Sas6 are recruited concomitantly and form the basic tubular structure of the centriole, followed by Sas4 recruitment which was shown to be important for the addition of the stabilizing centriole microtubules (Pelletier et al., 2006).

Centriole pairs display two distinct conjoined states: centriole cohesion and centriole engagement. Centriole cohesion is the tethering of centriole pairs via cohesion fibers and its freedom of separation is defined as less than or equal to two microns from each other (Mayor et al., 2000; Bahe et al., 2005; Yang et al., 2006) (Figure 1-1). Centriole engagement is the physical attachment of paired centrioles.

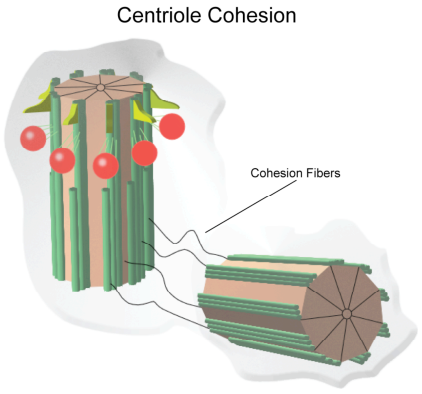


Figure 1-1. Centriole Cohesion
Cohesion fibers tether mother/daughter centriole pairs from the metaphase-to-anaphase transition until late G2 phase of the next cell cycle.

Engagement is initiated at daughter centriole inception in S-phase and remains in tact until disengagement occurs at the metaphase-to-anaphase transition of the ensuing mitosis (Tsou and Stearns, 2006b) (Figure 1-2).

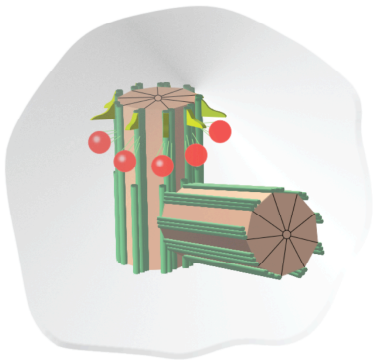


Figure 1-2. Centriole Engagement
The physical attachment of centrioles is engagement. Centriole engagement is established upon daughter centriole inception in S-phase and is maintained until disengagement occurs at the metaphase-to-anaphase transition.

### *Centriole Regulation*

After cell division, a cell inherits a pair of disengaged but cohered centrioles (Nigg, 2007). The centriole pair migrates to the

plasma membrane where the mother centriole functions as the basal body during primary cilium formation (Ishikawa et al., 2005; Bettencourt-Dias and Glover, 2007). Furthermore, the centriole pair also helps nucleate the interphase microtubule network. Centriole duplication commences at the G1- to S-phase transition where each centriole templates the assembly of a single daughter centriole that grows from its proximal base, in an engaged configuration. During G2-phase, the engaged centriole pairs remain

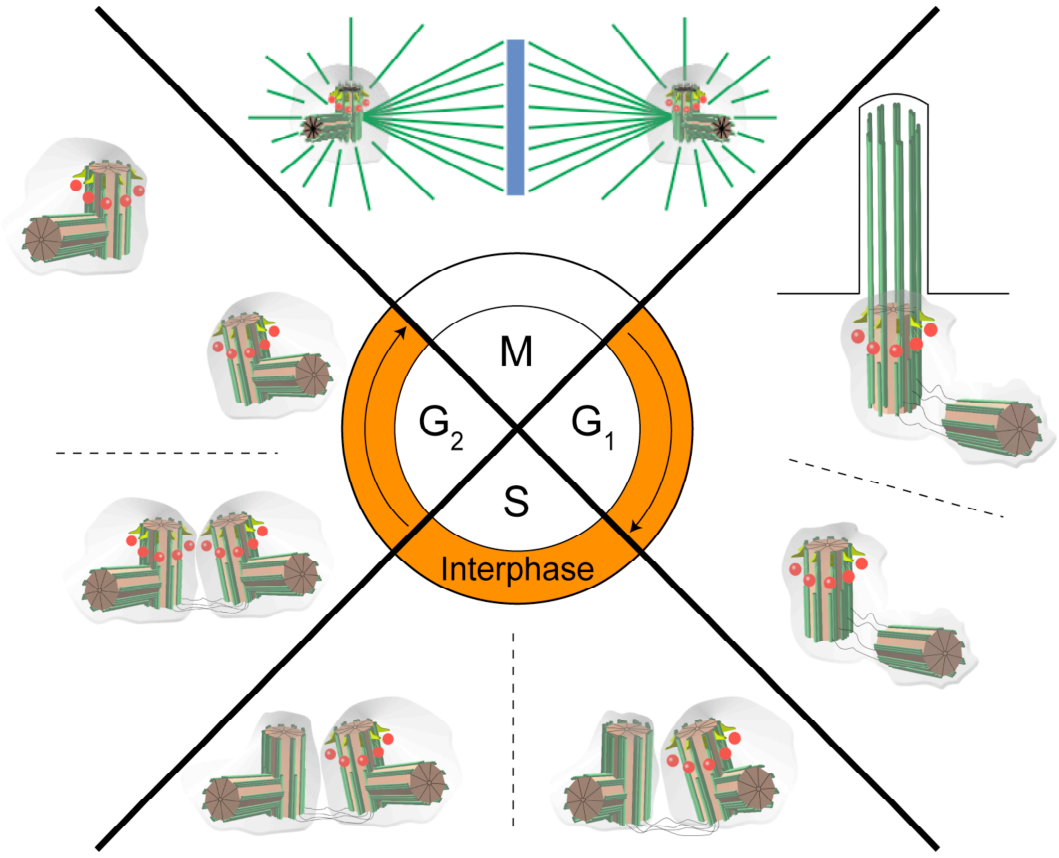


Figure 1-3. Centriole Duplication Cycle
Centriole disengagement occurs at the metaphase-to-anaphase transition. In G1, centrioles bound by centriole cohesion migrate to the plasma membrane where the mother centriole acts as the basal body for cilium formation. Centrioles duplicate in S-phase when daughter centrioles are templated from the proximal bases of each centriole. In G2, the daughter centriole inherited from the previous cell cycle matures into a mother centriole and centrosomes mature by assembling PCM. Late in G2, centriole cohesion is lost and centrosomes separate. In mitosis, centrosomes play a major role in nucleating the mitotic spindle.

tethered by cohesion fibers between the original inherited pair of centrioles (Mayor et al., 2000; Bahe et al., 2005; Yang et al., 2006). In G2-phase, the addition of distal and sub-distal appendages also ushers in the maturity of the oldest daughter centriole (the daughter centriole that served as a template) (Vorobjev and Chentsov Yu, 1982; Nakagawa et al., 2001; Ishikawa et al., 2005). Therefore, a "daughter-daughter" pair of centrioles is observed for a short period of time during the transition from S- to the G2-phase. At mitotic onset, centriole cohesion is lost coincident with centrosome migration to opposing ends of the cell where they are involved in the nucleation of the bipolar mitotic spindle (Faragher and Fry, 2003). Furthermore, PCM surrounding each centriole pair expands and the MTOC activity increase during mitosis. However, the mother-daughter centriole pair remains engaged until the metaphase-to-anaphase transition when engagement is lost in a separase-dependent manner (Tsou and Stearns, 2006b) (Figure 1-3).

Centriole duplication is a tightly regulated template-dependent process that occurs only once per cell cycle (Tsou and Stearns, 2006a; Azimzadeh and Bornens, 2007; Bettencourt-Dias and Glover, 2007; Nigg, 2007). Mechanisms that govern centriole duplication have begun to be elucidated (Tsou and Stearns, 2006a; Nigg, 2007; Strnad and Gonczy, 2008). Recent work has put forward a model that supports the loss of centriole engagement as the licensing step that allows centrioles to undergo a single round of duplication (Tsou and Stearns, 2006b, a; Nigg, 2007). This model purports that centriole disengagement, which occurs during the metaphase-to-anaphase transition, requires the actions of the protease, separase (Tsou and Stearns, 2006b). Centriole disengagement "licenses" centrioles to undergo a single round of duplication.

Conversely, while centrioles are engaged, centriole duplication is repressed thereby controlling centriole numbers. The putative licensing factor (i.e., target of separase) remains unknown.

Deregulation of the duplication cycle can lead to centrosome amplification, thereby increasing the frequency of multipolar spindles, likely leading to errors in chromosome segregation and aneuploidy (Brinkley, 2001; Pihan and Doxsey, 2003; Nigg, 2006). Whether centrosome amplification leads to aneuploidy remains unknown, however centrosome amplification is a hallmark of many cancers (Nigg, 2006). While excess centrosomes increase the probability of a cell assembling a multipolar spindle, an intrinsic centrosome clustering mechanism suppresses such occurrences (Sluder et al., 1997; Quintyne et al., 2005; Basto et al., 2008; Kwon et al., 2008; Yang et al., 2008). In the presence of multipolar spindles the mitotic checkpoint is activated, due to aberrant microtubule-kinetochore attachments, and allows cells ample time to cluster MTOCs into a pseudo-bipolar spindle (Basto et al., 2008; Kwon et al., 2008; Yang et al., 2008).

## B. Autosomal recessive primary microcephaly (MCPH): a centrosome-based disease?

### *Overview*

Increased brain size is a seminal event in human evolution, with a thousand-fold size difference observed between mouse and human (Northcutt and Kaas, 1995; Rakic, 1995). The human brain is strikingly bigger than that of primates and that increase gives strong precedence for the development of cognitive intelligence. Evolution has

accomplished this feat chiefly through enlargement of the cerebral cortices (Tang, 2006). However, the genetic alterations that have allowed humans to evolve a larger brain remain unknown. Atavistic alterations due to single gene mutations represent unique opportunities in the understanding of cellular mechanisms, disease, and human evolution.

Microcephaly is an atavistic condition resulting in a smaller than expected head circumference when compared to age- and sex-matched individuals, such measurements are later refined by more sensitive imaging methods such as magnetic resonance imaging (MRI) (Woods et al., 2005). The "small head" phenotype appears due to a volumetric reduction of the cranial cavity, but since the skull is expanded by brain growth during development the underlying cause is hypoplasia of the brain with the greatest impact found in the cerebral cortex. A sloping frontal and flatter occipital regions of the skull are common characteristics observed in affected individuals. Causes of microcephaly include genetic abnormalities as well as environmental factors including intrauterine infections, drug usage during pregnancy, prenatal radiation exposure, maternal phenylketonuria, and birth asphyxia all of which must be excluded before a diagnosis of MCPH can be considered (Cowie, 1960; Woods et al., 2005). However, genetic alterations remain the cause of the majority of the cases. Mircrocephaly is further divided into two subgroups: primary and secondary. Primary microcephaly is present at birth and results as a direct effect on brain development; secondary microcephaly develops post-natal, indicating a progressive neurodegenerative condition.

### *Brain Development*

The neocortex in the mammalian brain is a six-layered region generated from multiple rounds of neuronal progenitor cell divisions at the ventricular zone (Buchman and Tsai, 2007). This is an intricate process that relies on a fine balance of neuronal progenitor cells and generation of neurons and glial cells (Caviness et al., 1995). Neuronal progenitor cells are capable of both symmetric and asymmetric cell divisions. Progenitor cells undergo symmetric cell division to produce two identical daughter cells; divisions may be proliferative (progenitor → progenitor + progenitor) or neurogenic (progenitor → neuron + neuron) depending on expression of cell fate determinants within the dividing progenitor. Progenitors that divide via asymmetric cell division can produce two daughter cells with different cell fates (progenitor → progenitor + neuron). This is accomplished by segregating different differentiation factors into the distinct daughter cells. Importantly, the mammalian homologues of *Drosophila*, *Numb*, proteins that form crests during cell division have been shown to regulate the outcomes of divisions within the brain (Li et al., 2003).

Early in development neuronal progenitor cells use proliferative symmetric cell division to expand the progenitor population (progenitor → progenitor + progenitor). During neurogenesis progenitors utilize asymmetric cell divisions, allowing maintenance of neuronal progenitors while forming differentiated cells that will form the brain (progenitor → progenitor + neuron). Late in development, neuronal progenitors again utilize the symmetric cell division program to produce two differentiating daughters (progenitor → neuron + neuron), thereby eliminating the progenitor and its production potential.

*Autosomal Recessive Primary Microcephaly*

Autosomal recessive primary microcephaly (MCPH, [MIM 251200]), also referred to as "true microcephaly" or "microcephaly vera" is a genetic disorder that directly affects brain development (Jackson et al., 1998). Clinical features include a head circumference at least four standard deviations below age- and sex-means, mental retardation with no other neurological findings such as seizures or progressive cognitive decline; normal motor skills, height, weight, appearance, chromosome analysis, and brain scan (Woods et al., 2005). Mutations in seven loci (MCPH1-MCPH7) have been linked to MCPH. To date, mutations in five genes have been identified within these seven loci: *microcephalin* (*MCPH1*), *cyclin-dependent kinase 5 regulatory associated protein 2* (*CDK5RAP2, MCPH3*), *abnormal spindle-like microcephaly associated* (*ASPM, MCPH5*), *centromere associated protein J* (*SAS4/CPAP/CENPJ, MCPH6*), and *SCL/TAL1 interrupting locus* (*STIL, MCPH7*) (Bond et al., 2002; Jackson et al., 2002; Trimborn et al., 2004; Bond et al., 2005; Kumar et al., 2009). All five of the mapped MCPH genes encode centrosomal proteins, implicating a critical role for the centrosome in brain development (Bond et al., 2005; Zhong et al., 2005; Zhong et al., 2006; Pfaff et al., 2007). Interestingly, the essential centrosomal protein, pericentrin, has been linked to Seckel syndrome [MIM 210600] and microcephalic osteodysplastic primordial dwarfism type II (MOPD II, [MIM 210720]) (Griffith et al., 2008; Rauch et al., 2008). Like MCPH, Seckel syndrome and MOPD II are associated with smaller than normal brain size, suggesting a prominent role for the centrosome in control mechanisms that control organ size and overall stature.

**C. Scope of Dissertation**

The number of centrosomes within cells is directly influenced by the centriole duplication cycle. Although centrosome amplification is highly correlated with many cancers, mechanisms that control centriole duplication remain largely unknown. Our interest in characterizing the role of CDK5RAP2 in centrosome regulation was two-fold. Firstly, *CDK5RAP2* is one of two *centrosomin* (*cnn*) homologues in mammals. Secondly, truncating mutations in *CDK5RAP2* are linked to MCPH in humans. Since *Drosophila* Centrosomin (CNN) is involved in the formation of PCM we hypothesized that in mammals CDK5RAP2 would fulfill a similar role.

We derived two distinct mutant mouse lines expressing truncating mutations closely matching those found in humans to study CDK5RAP2 function. Upon close inspection of the mutant lines one was found to be a strong mutant, with no detection of full-length protein expression, while the other was a weak mutant and expressed a small amount of full-length CDK5RAP2. Furthermore, some of the phenotypes were observed only in the strong mutant line. Therefore, data are consistent with the weak mutant being a hypomorphic mutant.

Both weak and strong mutant cells showed defects in centriole cohesion. However, centriole amplification was limited to strong loss-of-function *CDK5RAP2* mutant mouse cells. Consequently, these cells frequently displayed multipolar spindles and were delayed in mitosis. In addition, excess mother centrioles promoted assembly of multiple primary cilia. Amplified centrioles were often disengaged and lost the normal centriole paired configuration. We propose that CDK5RAP2 is required to maintain

centriole engagement and cohesion. Because centriole disengagement is the key step in licensing centriole duplication, CDK5RAP2 is a negative regulator of centriole licensing. Thus, CDK5RAP2 restricts centriole duplication by maintaining centriole engagement.

# CHAPTER TWO

## ALTERED CENTROSOME REGULATION IN LOSS-OF-FUNCTION CDK5RAP2 MICE

### A. Introduction

Centrosome amplification poses a great risk to cells. Formation of multipolar spindles, due to multiple microtubule organizing centers (MTOCs), in mitosis has the potential to induce aneuploidy or cell death. Despite the cell's ability to cluster centrosomes, aneuploidy is highly possible due to syntelic attachments at kinetochores that can result during the clustering process.

Centrosomes are important organelles involved in a variety of processes. Regulating centriole formation regulates centrosome numbers within the cell. Recent studies have begun to unravel the intricacies of centriole duplication, however much still remains unknown. Furthermore, genetic studies have suggested that autosomal recessive primary microcephaly (MCPH), a human disease associated with reduced brain size, may be a centrosome-specific disease. Decoding the mechanisms that regulate the centriole cycle is an important endeavor that will further our understanding of the disease process in MCPH, correlation between cancer and centrosome amplification, and mechanisms involved in centrosome regulation within the cell.

**B. Results**

*CDK5RAP2 and Myomegalin are the Mammalian homologues of Drosophila Centrosomin*

Mammalian Cyclin-Dependent Kinase 5 Regulatory Associated Protein 2 (CDK5RAP2) and Myomegalin are members of the centrosomin family of proteins, conserved among eukaryotes from yeast to humans. While yeast and flies contain only one centrosomin family protein, mammals possess two. The founding member of this family, centrosomin (CNN), is required for mitotic centrosome function in *Drosophila melanogaster* (Megraw et al., 2001; Mahoney et al., 2006). The yeast *Schizosaccharomyces pombe* ortholog, Mto1p, is similarly required for MTOC functions (Sawin et al., 2004; Venkatram et al., 2004; Zimmerman and Chang, 2005). Both CDK5RAP2 and Myomegalin share homology with two domains in CNN, CNN motifs 1 and 2 (Figure 2-1). In flies, CNN is essential for the formation of the pericentriolar matrix (PCM); it is recruited to centrosomes at mitotic onset and maintains centrosomal localization throughout mitosis until its dissociation during cytokinesis (Li and Kaufman, 1996).

Myomegalin is a large centrosomal protein that has been implicated in the regulation of cyclic adenosine monophosphate (cyclic AMP) signaling (Verde et al., 2001). CDK5RAP2 is also a large centrosomal protein reported to be involved in centrosome cohesion and organization of the PCM (Graser et al., 2007; Fong et al., 2008).

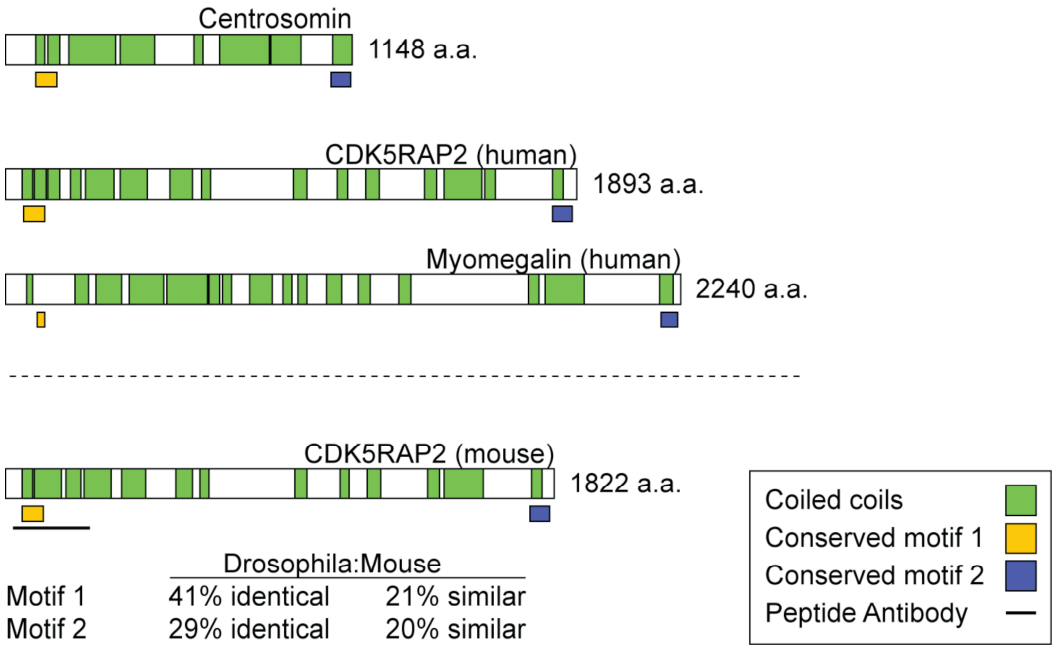


*Figure 2-1. Mammalian homologues of Drosophila Centrosomin*

Protein schematic comparing Drosophila centrosomin (CNN) with its putative human homologues: CDK5RAP2 and Myomegalin. Two conserved domains, each about 60 amino acids in length, are designated CNN conserved motifs 1 (Motif 1, orange box) and 2 (Motif 2, blue box). In addition to these conserved blocks, CNN family members contain extensive coiled-coil regions (green boxes). Mouse CDK5RAP2 is also shown along with identities and similarities between CNN and mCDK5RAP2 within Motifs 1 and 2. The black line indicates the antibody region.

It was discovered as an interacting partner of a Cyclin-Dependent Kinase 5 (CDK5) regulatory protein and is hypothesized to inhibit CDK5 function at the centrosome (Ching et al., 2000; Bond and Woods, 2006). We have focused our studies on the characterization of *CDK5RAP2*.

### *Centrosome levels of CDK5RAP2 change with the cell cycle*

In order to determine if CDK5RAP2 functioned in a similar manner as CNN and to investigate its relationship with the centrosome we examined its subcellular localization and dynamics. To do this, antibodies were produced against the amino-terminal end of CDK5RAP2 (Figure 2-1, black line). Immunofluorescence staining of NIH-3T3 cells, an immortalized mouse embryo fibroblasts cell line, showed that CDK5RAP2 is a centrosomal protein (Figure 2-2A), consistent with previous reports (Bond et al., 2002; Graser et al., 2007; Fong et al., 2008). Furthermore, when cells were treated with nocodazole, to destabilize microtubules, CDK5RAP2's centrosome localization remained unchanged showing that localization was not microtubule dependent (Figure 2-5A). An amino-terminal green fluorescent protein conjugation construct (GFP-CDK5RAP2) transiently transfected into NIH-3T3 cells also localized to centrosomes (Figure 2-2B) showing that the conjugation of the green fluorescent protein did not disrupt CDK5RAP2 localization. Next, changes in CDK5RAP2 levels at centrosomes throughout the cell cycle were examined in NIH-3T3 cells. Interphase centrosomes showed relatively low levels of CDK5RAP2, however levels were observed to increase at prophase of mitosis, and remained high throughout the ensuing stages of

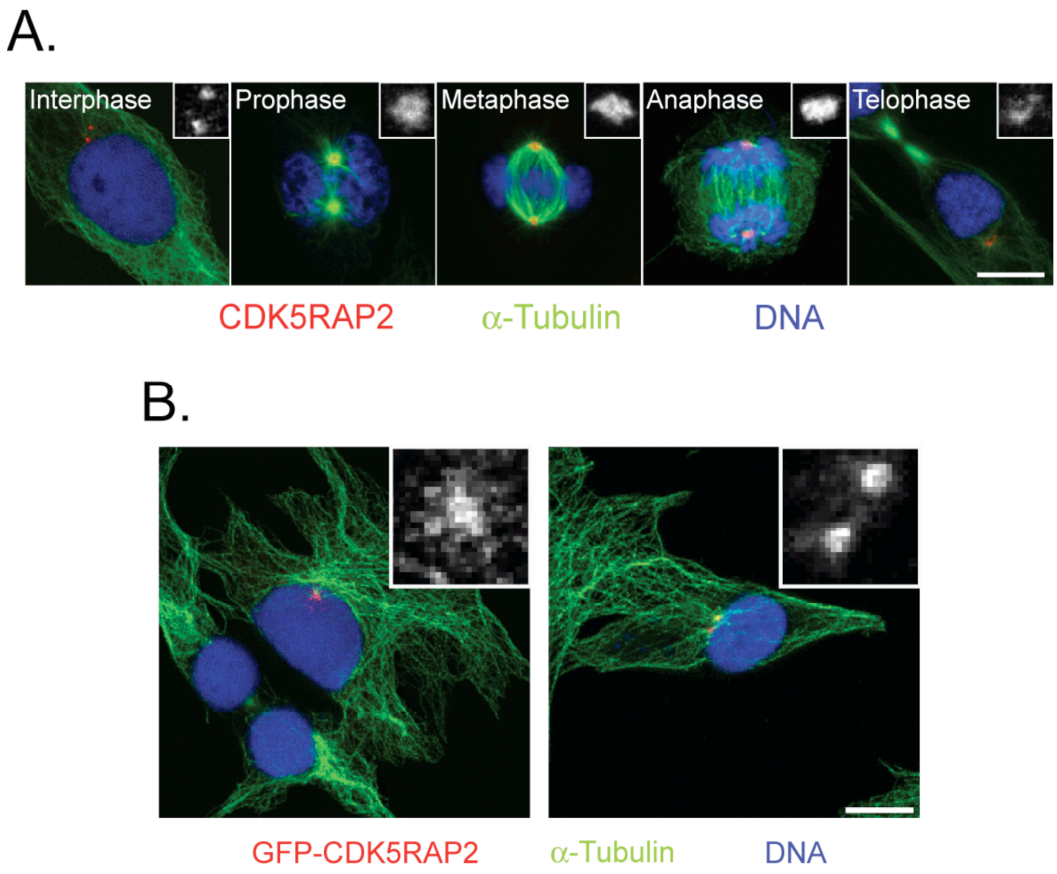


*Figure 2-2. CDK5RAP2 localizes to centrosomes in mammalian cells*

(A) CDK5RAP2 centrosomal levels change with the cell cycle. Immunofluorescence images of NIH-3T3 mouse fibroblasts stained for CDK5RAP2 (red), α-tubulin (green), and DNA (blue) at different stages of the cell cycle. Insets are enlargements of CDK5RAP2 signal to highlight changes in CDK5RAP2 levels at centrosomes. During mitosis, CDK5RAP2 levels increase through anaphase and decrease again at telophase. (B) GFP-tagged CDK5RAP2 localizes to centrosomes. NIH-3T3 cells were transiently transfected with a GFP-CDK5RAP2 expressing plasmid. Immunofluorescence images of cells stained for GFP (red), α-Tubulin (green), and DNA (blue). Insets are enlarged images of the GFP signal at the centrosome. Scale bars = 10μm.

mitosis until telophase, when levels dropped to those initially observed in interphase (Figure 2-2A).

While CDK5RAP2 is a centriolar resident (Graser et al., 2007; Fong et al., 2008), our results show that CDK5RAP2 accumulates at centrosomes, consistent with localization to the PCM, which grows at mitosis (Palazzo et al., 2000). Thus, CDK5RAP2 is a centrosomal protein whose centrosomal levels are regulated in a cell cycle-dependent manner. Because CDK5RAP2 is a centrosomal protein whose mutation causes disease, we next examined the function of CDK5RAP2 in mammalian cells.

*Generation of CDK5RAP2 mutant mice*

To further understand CDK5RAP2's role in centrosome biology and MCPH, we derived mutant mice using two Bay genomics embryonic stem cell clones, RRU031 and RRF465, harboring splice-trap insertions within introns 3 and 12 of the *CDK5RAP2* locus, respectively. The splice-trap vector used to generate the *CDK5RAP2* mutations contains a superior splice site upstream of a "β-Geo" fusion cassette, a fusion between the β-galactosidase and neomycin phosphotransferase sequence (Stryke et al., 2003). In $CDK5RAP2^{Gt(RRU031)Byg/Gt(RRU031)Byg}$ and $CDK5RAP2^{Gt(RRF465)Byg/Gt(RRF465)Byg}$ mutant mice (hereafter referred to as $CDK5RAP2^{RRU031/RRU031}$ and $CDK5RAP2^{RRF465/RRF465}$, respectively), the splice traps result in translation of the first 64 and 435 amino acids of CDK5RAP2, respectively, fused to β-Geo (Figure 2-3A,C). The truncated proteins expressed from these *CDK5RAP2* alleles are similar to the predicted protein products of the human *CDK5RAP2* mutations, S81X and E385fsX4, which result in truncated proteins of 81 and 389 amino acids, respectively (Figure 2-3A,C) (Bond et al., 2005).

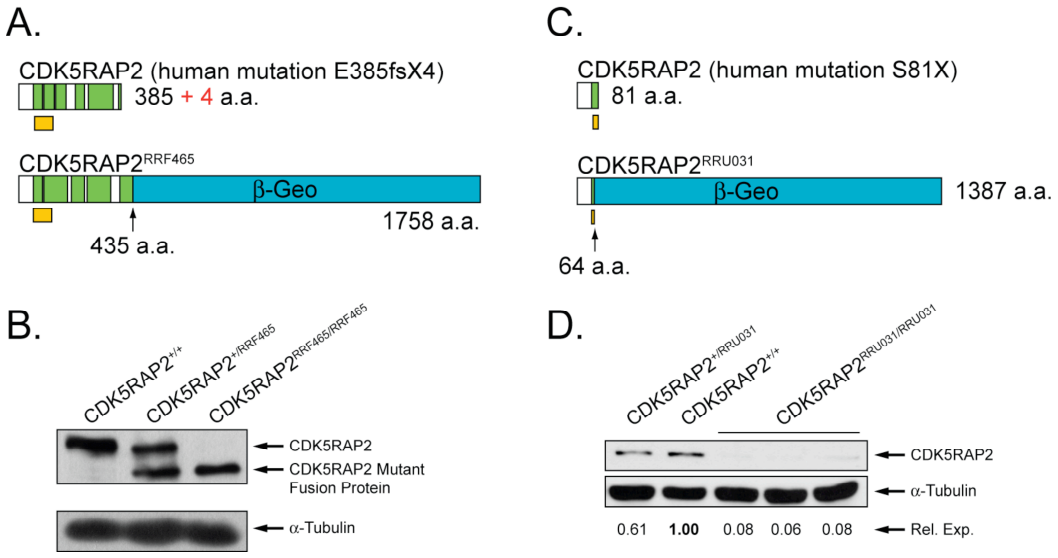


*Figure 2-3. CDK5RAP2 mutant mice express truncated protein products*

(A) The truncated CDK5RAP2 product expressed in *CDK5RAP2*$^{RRF465/RRF465}$ mice is similar to the human mutation, E385fsX4 (Bond et al., 2005). Schematic compares the human and mouse protein products resulting from these mutations.
(B) Western blot of whole cell lysates collected from sibling *CDK5RAP2*$^{RRF465/RRF465}$ MEF cultures of all three genotypes probed, with CDK5RAP2 antibodies. *CDK5RAP2*$^{+/+}$ and *CDK5RAP2*$^{+/RRF465}$ MEFs express full-length CDK5RAP2 protein while *CDK5RAP2*$^{+/RRF465}$ and *CDK5RAP2*$^{RRF465/RRF465}$ MEFs express the CDK5RAP2 mutant fusion protein produced by the splice-trap insertion.
(C) The truncated CDK5RAP2 protein expressed in *CDK5RAP2*$^{RRU031/RRU031}$ mice is similar to the human mutation, S81X (Bond et al., 2005). Schematic compares the human and mouse protein products resulting from these mutations.
(D) Western blot of whole cell lysates collected from sibling *CDK5RAP2*$^{RRU031/RRU031}$ MEF cultures. Full-length CDK5RAP2 was expressed in *CDK5RAP2*$^{+/RRU031}$ MEFs at approximately 61% of the levels in *CDK5RAP2*$^{+/+}$ MEFs. While *CDK5RAP2*$^{RRU031/RRU031}$ MEFs retained residual full-length CDK5RAP2 expression, approximately 7% of *CDK5RAP2*$^{+/+}$ MEF levels. Thus, the RRU031 insertion splice trap is leaky and results in a hypomorphic mutation. CDK5RAP2 expression was quantified using Image J software and is shown relative to wild-type. In western blots, α-tubulin was probed as a loading control.

Homozygous mutants from both *CDK5RAP2* lines were viable and born at expected mendelian ratios. Female *CDK5RAP2*$^{RRF465/RRF465}$ mice were fertile (n=5). Males, however, showed variable fertility, with 2 out of 6 mice showing severe infertility (n=6). Brain size was assessed by comparing brain versus body weight and by H&E staining of coronal brain sections. Neither group of CDK5RAP2 mutant mice showed evidence of reduced brain size (Table 2-1 and Figure 2-4).

In order to investigate CDK5RAP2 functions in centrosome structure and regulation at the cellular level, mouse embryonic fibroblasts (MEFs) were derived from embryonic day E14.5 embryos. Wild-type littermates served as controls. We characterized differences in CDK5RAP2 expression between the two mutant lines using the affinity-purified antibody. The region used to raise antibodies was retained in the *CDK5RAP2*$^{RRF465/RRF465}$ mutant fusion protein (Figures 2-1 and 2-3A). Western blot analysis using whole cell lysates showed that *CDK5RAP2*$^{+/+}$ MEFs expressed full-length CDK5RAP2, heterozygous *CDK5RAP2*$^{+/RRF465}$ MEFs expressed both full-length CDK5RAP2 and CDK5RAP2 mutant fusion protein, and homozygous *CDK5RAP2*$^{RRF465/RRF465}$ MEFs expressed only the CDK5RAP2 mutant fusion protein (Figure 2-3B). Furthermore, the mutant fusion protein produced in *CDK5RAP2*$^{RRF465/RRF465}$ MEFs maintained centrosomal localization, although slight differences did exist when compared to *CDK5RAP2*$^{+/+}$ *MEFs* (Figure 2-5A, see below). On the other hand, we were able to detect only full-length CDK5RAP2 protein in *CDK5RAP2*$^{RRU031}$ MEFs. However, we observed that *CDK5RAP2*$^{+/RRU031}$ MEFs expressed 61% full-length protein compared to wild-type controls while

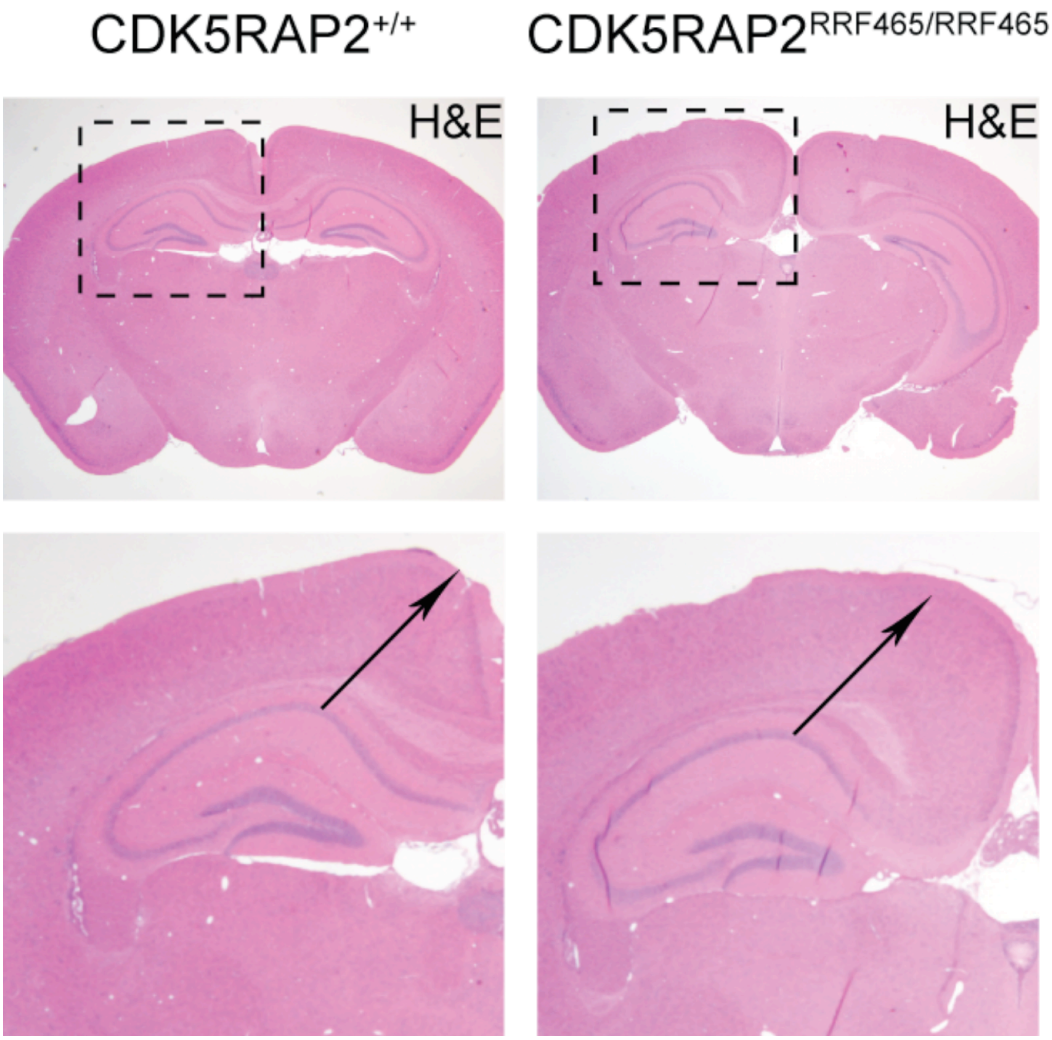


*Figure 2-4. CDK5RAP2 mutant mice do not develop microcephaly*

Hematoxylin and Eosin stained coronal sections from *CDK5RAP2*$^{+/+}$ and *CDK5RAP2*$^{RRF465/RRF465}$ brains. Brain sections were from closely matched regions. Arrows are at the same angle and of the same length and illustrate the similar cerebral cortex thickness between the wild-type and mutant mice. No overt differences were observed in cerebral size, thickness, or morphology. Enlarged images correspond to boxed area.

| Table 2-1 | *CDK5RAP2*$^{+/+}$ | *CDK5RAP2*$^{RRU031/RRU031}$ | *CDK5RAP2*$^{RRF465/RRF465}$ |
|---|---|---|---|
| Avg. body weight | 37.6 g | 29.3 g | 37.6 g |
| Avg. brain weight | 554.6 mg | 515 mg | 527.5 mg |
| brain/body ratio | 14.9 | 18.5 | 14.2 |
| n | 5 | 2 | 5 |

*CDK5RAP2*$^{RRU031/RRU031}$ MEFs expressed approximately 7% full-length CDK5RAP2, some or all of which was localized at centrosomes (Figure 2-3D). Therefore, the RRU031 mutation is leaky and hypomorphic, which can occur in splice trap mutants when the genetic trap is spliced out during mRNA processing. These results reveal differences in the relative strengths of the two splice trap mutations, and establish the first mouse mutant models of MCPH and of the centrosomin family of centrosomal proteins.

The centrosome phenotypes described below support the observations that the *CDK5RAP2*$^{RRU031/RRU031}$ mutant is a hypomorphic mutation, expressing a low amount of full-length CDK5RAP2, and that the *CDK5RAP2*$^{RRF465/RRF465}$ mutant is more severe.

### *Loss of CDK5RAP2 affects centrosome structure*

The *CDK5RAP2*$^{RRF465/RRF465}$ protein was stable (Figure 2-3B), and retained centrosome localization (Figure 2-5A). From these data we conclude that the first 435 amino acids of CDK5RAP2 are sufficient for centrosomal localization. However, full-length CDK5RAP2 and the mutant fusion protein in *CDK5RAP2*$^{RRF465/RRF465}$ MEFs exhibited different localization within centrosomes. Full-length CDK5RAP2 localized to centrioles and also to fibrous projections that emanated from the centrosome (PCM fibers). These PCM fibers were not microtubules or microtubule-dependent, as localization of CDK5RAP2 to these structures persisted upon microtubule disassembly with nocodazole (Figures 2-5A). The CDK5RAP2 mutant fusion protein expressed in *CDK5RAP2*$^{RRF465/RRF465}$ MEFs retained centriole localization yet failed to localize to PCM

fibers (Figure 2-5A). Thus, the normal PCM architecture of centrosomes was disrupted in *CDK5RAP2*$^{RRF465/RRF465}$ MEFs.

These slight differences in localization prompted us to look at localization of other centrosomal proteins in *CDK5RAP2*$^{RRF465/RRF465}$ MEFs, and found that rootletin, a cohesion fiber protein (Bahe et al., 2005), co-localized with CDK5RAP2 at PCM fibers in *CDK5RAP2*$^{+/+}$ MEFs (Figure 2-5B). Here again, nocodazole treatment demonstrated that co-localization of CDK5RAP2 and rootletin at PCM fibers was not microtubule-dependent (Figure 2-5B). However, in *CDK5RAP2*$^{RRF465/RRF465}$ MEFs, rootletin was mis-localized from PCM fibers mirroring the mis-localization of the CDK5RAP2 mutant fusion protein (Figure 2-5C). When rootletin localization was assessed in both mutant MEF lines we found that indeed, rootletin localization to PCM fibers was disrupted in *CDK5RAP2*$^{RRF465/RRF465}$ MEFs and, to a lesser and variable degree, also in *CDK5RAP2*$^{RRU031/RRU031}$ MEFs (Figures 2-6A). While rootletin localization to PCM fibers was completely disrupted in *CDK5RAP2*$^{RRF465/RRF465}$ MEFs, the incidence of weak rootletin signal at PCM fibers or reduced number of PCM fibers increased more than 2-fold in *CDK5RAP2*$^{RRU031/RRU031}$ MEFs (*CDK5RAP2*$^{+/+}$: 28% vs. *CDK5RAP2*$^{RRU031/RRU031}$: 66%) (Figure 2-6B). These results show that CDK5RAP2 regulates assembly of a cohesion fiber protein, consistent with the requirement for CDK5RAP2 in centrosome cohesion (see below and Graser et al., 2007). Interestingly, PCM fibers were not prominent in all mouse cells; centrosomes in NIH-3T3 cells, an immortalized mouse embryo fibroblast cell line, did not display these structures as elaborately (Figure 2-2). Nevertheless, disruption of rootletin localization shows that centrosome structure is altered in *CDK5RAP2* mutant MEFs. In contrast, *CDK5RAP2* mutant MEFs showed

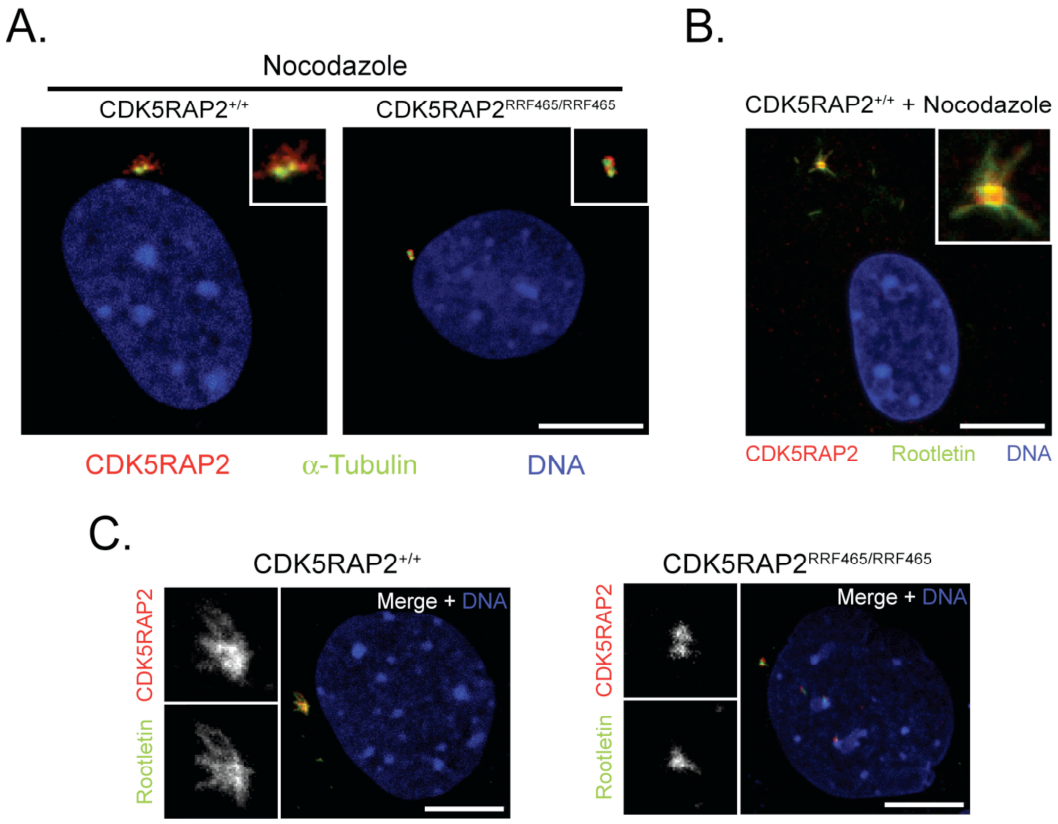


*Figure 2-5. CDK5RAP2 and rootletin co-localize at PCM fibers*

(A) CDK5RAP2 localization to PCM fibers is not microtubule dependent. Immunofluorescence images of nocodazole-treated *CDK5RAP2*$^{+/+}$ and *CDK5RAP2*$^{RRF465/RRF465}$ MEFs stained for CDK5RAP2 (red), α-tubulin (green), and DNA (blue).
(B) CDK5RAP2 and rootletin co-localization at PCM fibers is not microtubule-dependent. Immunofluorescence images of nocodazole-treated *CDK5RAP2*$^{+/+}$ MEFs stained for CDK5RAP2 (red), rootletin (green), and DNA (blue). Inset shows an enlargement of CDK5RAP2 and rootletin at the centrosome region.
(C) CDK5RAP2 and rootletin co-localization is lost in *CDK5RAP2*$^{RRF465/RRF465}$ MEFs. Immunofluorescence images of *CDK5RAP2*$^{+/+}$ and *CDK5RAP2*$^{RRF465/RRF465}$ MEFs stained for CDK5RAP2 (red), rootletin (green), and DNA (blue). CDK5RAP2 and rootletin co-localize to centrioles and PCM fibers. Enlargements are of the centrosome region. Scale bars = 10 μm.

normal centrosomal localization of cenexin/ODF2, centrobin, centrin, γ-tubulin, pericentrin, TOG, aurora-A, and EB1 (Figures 2-3A and 2-8A; TOG, aurora-A and EB1 not shown).

### *CDK5RAP2 restricts centriole duplication*

Centrosome amplification was a prominent feature of *CDK5RAP2*$^{RRF465/RRF465}$ MEFs. Immunofluorescence staining for γ-tubulin (PCM marker) and centrin (centriole marker) showed that *CDK5RAP2*$^{+/+}$ MEFs contained one or two pairs of centrin puncta, representing normal centriole complements in G1- and G2-phase, respectively (Figure 2-7A). In contrast, a high percentage of *CDK5RAP2*$^{RRF465/RRF465}$ MEFs had greater than normal centrin and γ-tubulin puncta, showing that these cells had amplified centrioles that could organize PCM (Figure 2-7A and see below).

*CDK5RAP2*$^{RRF465/RRF465}$ MEFs had a greater than 4-fold increase of cells with three centrioles (*CDK5RAP2*$^{+/+}$: 2.5% vs. *CDK5RAP2*$^{RRF465/RRF465}$: 11.2%), and a greater than 5-fold increase in cells with more than four centrioles (*CDK5RAP2*$^{+/+}$: 4.2% vs. *CDK5RAP2*$^{RRF465/RRF465}$: 22.0%). These increased values were accompanied by reciprocal decreases in MEFs containing two centrioles (*CDK5RAP2*$^{+/+}$: 85.0% vs. *CDK5RAP2*$^{RRF465/RRF465}$: 49.8%) (Figure 2-7B). Heterozygous RRF465 MEFs were similar to *CDK5RAP2*$^{+/+}$ MEFs and only 2% of cells had greater than four centrioles (data not shown). Therefore, the RRF465 gene trap allele is not a dominant mutation in *CDK5RAP2*. Overall, 33.2% of *CDK5RAP2*$^{RRF465/RRF465}$ MEFs, exhibited amplified

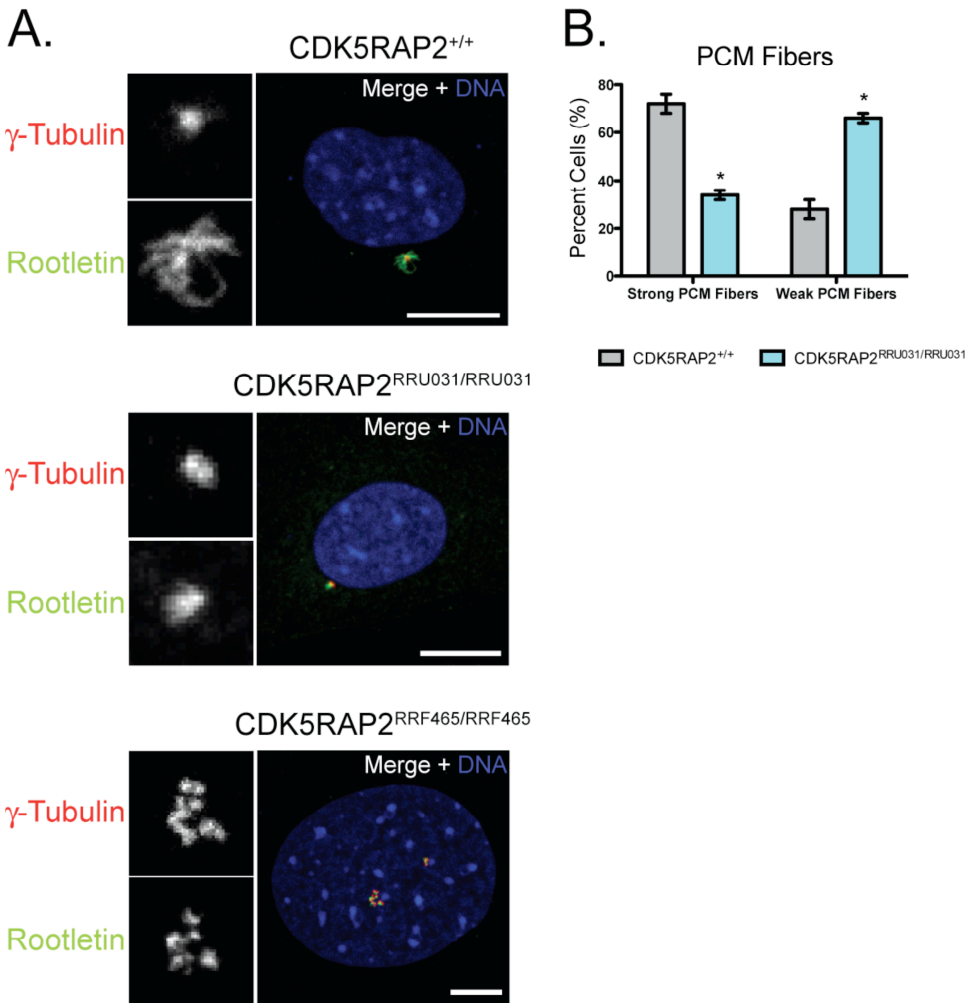


*Figure 2-6. PCM fibers are affected in CDK5RAP2 mutant MEFs*

(A) Immunofluorescence images of *CDK5RAP2*$^{+/+}$, *CDK5RAP2*$^{RRU031/RRU031}$, and *CDK5RAP2*$^{RRF465/RRF465}$ MEFs stained for γ-tubulin (red), rootletin (green), and DNA (blue). Rootletin localized strongly to centrioles and PCM fibers in *CDK5RAP2*$^{+/+}$, in *CDK5RAP2*$^{RRU031/RRU031}$ localization is decreased and fewer PCM fibers form, and localization to PCM fibers is lost in *CDK5RAP2*$^{RRF465/RRF465}$ MEFs. Enlargements are of the centrosome region. Scale bars = 10 μm.
(B) *CDK5RAP2*$^{RRU031/RRU031}$ MEFs are deficient in PCM fiber formation. Comparison of strong PCM fiber (*CDK5RAP2*$^{+/+}$: 72% ± 4% vs. *CDK5RAP2*$^{RRU031/RRU031}$: 34% ± 2%, $p<0.05$) versus weak PCM fiber (*CDK5RAP2*$^{+/+}$: 28% ± 4% vs. *CDK5RAP2*$^{RRU031/RRU031}$: 66% ± 2%, $p<0.05$) formation in *CDK5RAP2*$^{+/+}$ and *CDK5RAP2*$^{RRU031/RRU031}$ MEFs. Examples in (A) represent strong, weak and ablated PCM fibers. n = 50 cells total from two independent cell lines. Error bars represent standard error of the means (SEM).

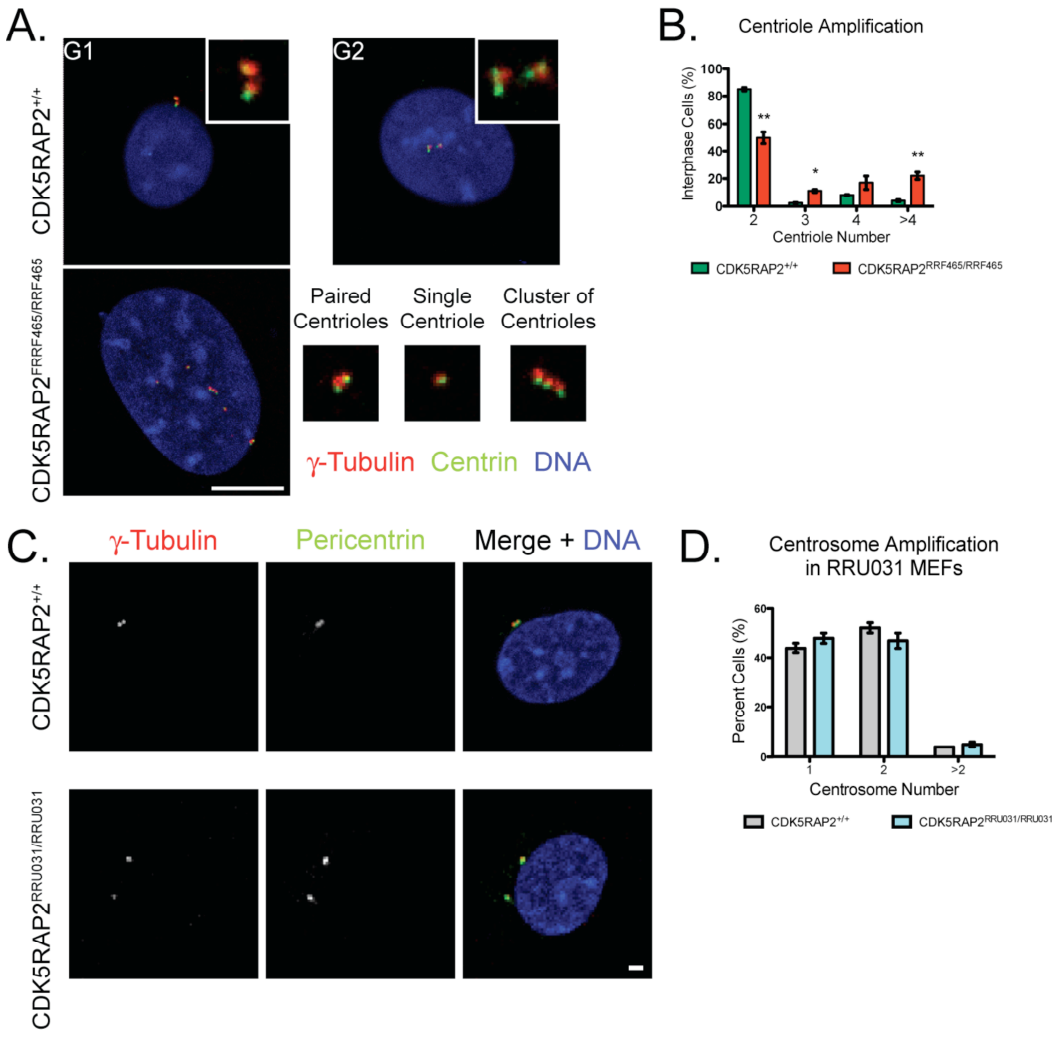


*Figure 2-7. CDK5RAP2 restricts centriole duplication*

(A) *CDK5RAP2*$^{RRF465/RRF465}$ MEFs have amplified centrioles that form aberrant centriole configurations, including singlets and singlet clusters. Immunofluorescence images of *CDK5RAP2*$^{+/+}$ and *CDK5RAP2*$^{RRF465/RRF465}$ MEFs stained for γ-tubulin (red), the centriole marker centrin (green), and DNA (blue). Paired centrioles in G1- and G2-phase *CDK5RAP2*$^{+/+}$ MEFs are shown. The example *CDK5RAP2*$^{RRF465/RRF465}$ MEF shows three singlet centrioles, one apparent pair, and a cluster of three. Enlargements of each are shown on the right. Scale bar = 10 μm.

(B) Quantification of cells with 2, 3, 4, or greater than 4 centrioles in *CDK5RAP2*$^{+/+}$ (green bars) and *CDK5RAP2*$^{RRF465/RRF465}$ (red bars) cells. MEFs containing 2 centrioles (CDK5RAP2$^{+/+}$: 85.0% ± 1.3% vs. *CDK5RAP2*$^{RRF465/RRF465}$: 49.8% ± 2.5%, $p<0.01$), 3 centrioles (CDK5RAP2$^{+/+}$: 2.5% ± 0.3% vs. *CDK5RAP2*$^{RRF465/RRF465}$: 11.2% ± 0.6%, $p<0.05$), 4 centrioles (CDK5RAP2$^{+/+}$: 8.3% ± 0.3% vs. *CDK5RAP2*$^{RRF465/RRF465}$: 17% ± 2.8%, $p>0.05$), and greater than 4 centrioles (CDK5RAP2$^{+/+}$: 4.2% ± 0.7% vs. *CDK5RAP2*$^{RRF465/RRF465}$: 22.0% ± 1.5%, $p<0.005$). Data were collected from 3 independent experiments, n = 200 cells per experiment. Error bars represent SEM.
(C) Immunofluorescence images of *CDK5RAP2*$^{+/+}$ and *CDK5RAP2*$^{RRU031/RRU031}$ MEFs stained for γ-tubulin (left, red in merged panel), pericentrin (middle, green in merged panel), and DNA (blue in merged panel). Note the increased distance between the centrosomes in the mutant cell. Scale bar = 2μm.
(D) Centrosome amplification was not observed in *CDK5RAP2*$^{RRU031/RRU031}$ MEFs compared to *CDK5RAP2*$^{+/+}$ MEFs. Quantification of 1, 2, or greater than 2 centrosomes in *CDK5RAP2*$^{+/+}$ (gray bars) and *CDK5RAP2*$^{RRU031/RRU031}$ (cyan bars) cells demonstrated no centrosome amplification in mutant cells. MEFs containing 1 centrosome (*CDK5RAP2*$^{+/+}$: 44% ± 2.0% vs. *CDK5RAP2*$^{RRU031/RRU031}$: 48% ± 2.0%, $p>0.05$), 2 centrosomes (*CDK5RAP2*$^{+/+}$: 52% ± 2.0% vs. *CDK5RAP2*$^{RRU031/RRU031}$: 47% ± 3.0%, $p>0.05$), or greater than 2 centrosomes (*CDK5RAP2*$^{+/+}$: 4.0% ± 0% vs. *CDK5RAP2*$^{RRU031/RRU031}$: 5.0% ± 1.0%, $p>0.05$). n = 100 cells total from two independent cell lines. Error bars represent SEM.

centrioles, compared to only 6.7% of *CDK5RAP2*$^{+/+}$ MEFs. Thus, *CDK5RAP2*$^{RRF465/RRF465}$ MEFs exhibited aberrant regulation of centriole duplication, resulting in centriole amplification. In contrast, no centrosome amplification was observed in *CDK5RAP2*$^{RRU031/RRU031}$ MEFs, an indication that only a small amount of full-length CDK5RAP2 is sufficient to restrict centriole duplication (Figure 2-7C,D).

To assess mother and daughter centriole populations in *CDK5RAP2*$^{RRF465/RRF465}$ MEFs, we co-stained for the mother specific, cenexin/ODF2 and the daughter centriole-specific marker, centrobin (Figure 2-8A). These results showed that mother and daughter centrioles were both amplified in *CDK5RAP2*$^{RRF465/RRF465}$ MEFs (Figure 2-8B). Daughter centriole numbers exceeded those of mother centrioles, consistent with a model that centriole engagement is lost prematurely and multiple rounds of daughter synthesis occur in each cell cycle.

Centrosome amplification was also observed *in vivo* in *CDK5RAP2*$^{RRF465/RRF465}$ embryonic mice. Centrosomes were counted in coronal sections of the cerebral cortex of E14.5 embryonic brains. Immunofluorescence staining for pericentrin and actin was used to identify centrosomes and cell boundaries, respectively. Centrosomes were amplified in cells of the embryonic frontal cortex *in vivo*, similar to what was found in primary MEF cultures (Figure 2-9A). There was a 7-fold increase in the percent of *CDK5RAP2*$^{RRF465/RRF465}$ cells that contained more than two centrosomes compared to wild-type cells (*CDK5RAP2*$^{+/+}$: 3.3% vs. *CDK5RAP2*$^{RRF465/RRF465}$: 23.3%) (Figure 2-9B). These data indicate that centrosome amplification occurs *in vivo* in *CDK5RAP2*$^{RRF465/RRF465}$ mice at levels slightly less than but similar to what we observed in cultured MEFs.

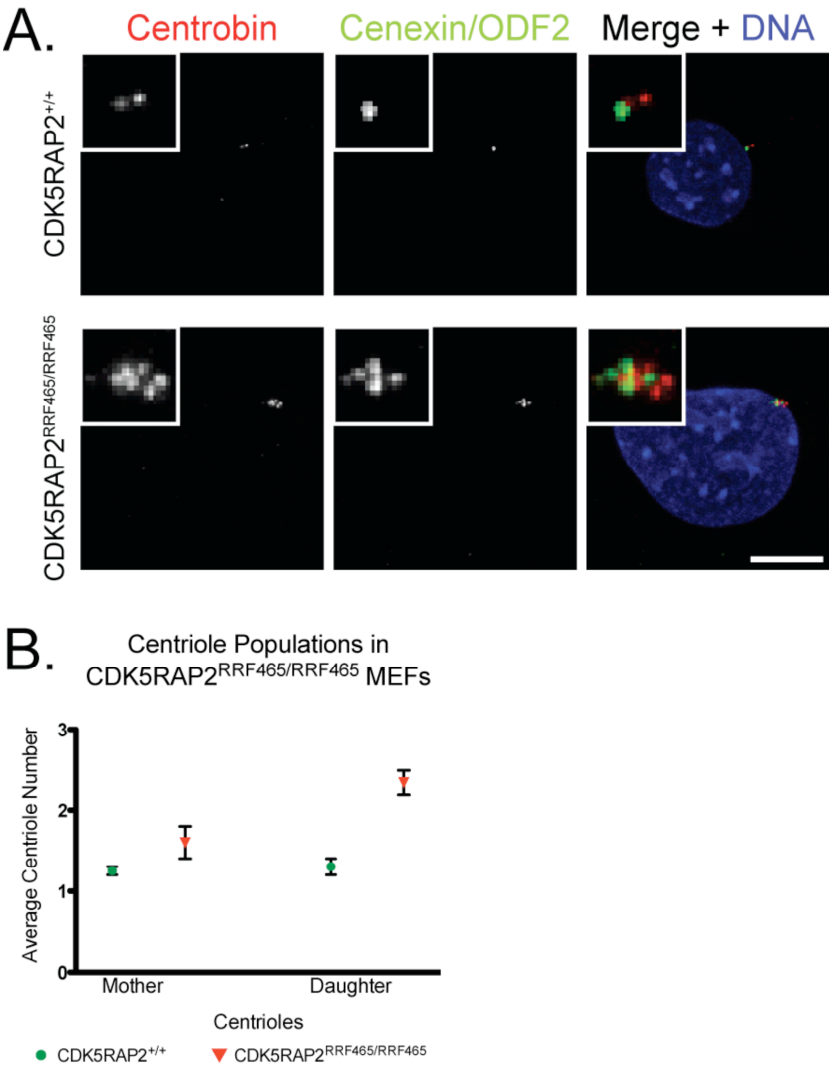


*Figure 2-8. Both mother and daughter centriole populations are amplified in* $CDK5RAP2^{RRF465/RRF465}$ *MEFs*

(A) Immunofluorescence images of $CDK5RAP2^{+/+}$ and $CDK5RAP2^{RRF465/RRF465}$ MEFs stained with the daughter centriole specific marker, centrobin (left, red in merged panel), the mother centriole specific marker, cenexin/ODF2 (middle, green in merged panel), and DNA (blue in merged panel). Examples show a $CDK5RAP2^{+/+}$ cell containing a pair of centrioles (one mother and one daughter) and a $CDK5RAP2^{RRF465/RRF465}$ cell that contains amplified mother and daughter centrioles. Insets show enlargements of the centriole region. Scale bar = 10 μm.

(B) Dot plot of the average number of mother ($CDK5RAP2^{+/+}$: 1.3 ± 0.05 vs. $CDK5RAP2^{RRF465/RRF465}$: 1.6 ± 0.2) and daughter ($CDK5RAP2^{+/+}$: 1.3 ± 0.1 vs. $CDK5RAP2^{RRF465/RRF465}$: 2.4 ± 0.15) centrioles per cell. Both centriole populations were increased in $CDK5RAP2^{RRF465/RRF465}$ MEFs. However, daughter centrioles were amplified more than mother centrioles. In these experiments, MEFs were blocked in G1-phase by serum starvation. Data were collected from three independent experiments, n = 90 cells total. Error bars represent SEM.

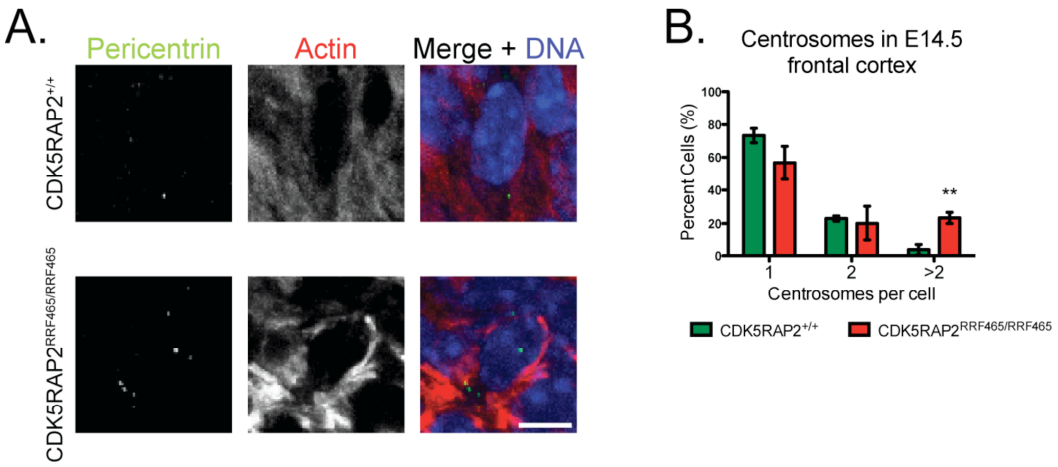


*Figure 2-9. CDK5RAP2 restricts centriole duplication in vivo*

(A) Immunofluorescence images of E14.5 coronal brain sections from *CDK5RAP2*$^{+/+}$ and *CDK5RAP2*$^{RRF465/RRF465}$ mice stained for pericentrin (left, green in merged panel), actin (middle, red in merged panel), and DNA (blue in merged panel). Centrosome amplification was observed in a significantly greater percentage of *CDK5RAP2*$^{RRF465/RRF465}$ cells than in the *CDK5RAP2*$^{+/+}$ cells. Scale bar = 10 μm.
(B) Quantification of cells with 1 (*CDK5RAP2*$^{+/+}$: 73.3% ± 4.4% vs. *CDK5RAP2*$^{RRF465/RRF465}$: 56.7% ± 10.1%, $p>0.05$), 2 (*CDK5RAP2*$^{+/+}$: 23.3% ± 1.7% vs. *CDK5RAP2*$^{RRF465/RRF465}$: 20% ± 10.4%, $p>0.05$), or greater than 2 (*CDK5RAP2*$^{+/+}$: 3.3% ± 3.3% vs. *CDK5RAP2*$^{RRF465/RRF465}$: 23.3% ± 3.3%, $p<0.0005$) centrosomes in *CDK5RAP2*$^{+/+}$ (green bars) and *CDK5RAP2*$^{RRF465/RRF465}$ (red bars) cells. Data were collected from 3 coronal sections, n = 300 cells total. Error bars represent SEM.

*Centriole amplification in CDK5RAP2$^{RRF465/RRF465}$ MEFs is associated with increased nuclear size*

Another salient phenotype of *CDK5RAP2$^{RRF465/RRF465}$* MEFs was the presence of enlarged nuclei. Frequently, the nuclear diameter was increased approximately 3-fold (Figure 2-7A). Quantification of nuclear size across cultures revealed a small but significant increase in the average nuclear area of *CDK5RAP2$^{RRF465/RRF465}$* MEFs (*CDK5RAP2$^{+/+}$*: 230.3 μm$^2$ vs. *CDK5RAP2$^{RRF465/RRF465}$*: 262.0 μm$^2$). However, the mean nuclear area was significantly larger, 528.0 μm$^2$, among *CDK5RAP2$^{RRF465/RRF465}$* MEFs with amplified centrioles (Figure 2-10A). Since centriole amplification and increased DNA content would coincide if cytokinesis failed, we measured DNA content of *CDK5RAP2$^{+/+}$* and *CDK5RAP2$^{RRF465/RRF465}$* MEFs. DNA analysis by flow cytometry revealed no increase of polyploid cells in *CDK5RAP2$^{RRF465/RRF465}$* MEFs, nor did we observe an increase of binucleate cells to indicate cytokinesis defects (Figure 2-11). In addition, we compared the fluorescence signal of the nuclear stain, 4',6-diamidino-2-phenylindole (DAPI), between *CDK5RAP2$^{+/+}$* and *CDK5RAP2$^{RRF465/RRF465}$* MEFs with amplified centrosomes, and compared this to wild-type binucleate cells as a tetraploid control. Binucleate cells had an approximately 2-fold increase in DAPI signal compared to *CDK5RAP2$^{+/+}$* or *CDK5RAP2$^{RRF465/RRF465}$* MEFs with amplified centrosomes (Figure 2-10B). Although there was a slight increase in DAPI signal between MEFs with one or two centrosomes and those with greater than two centrosomes the differences were not significant.

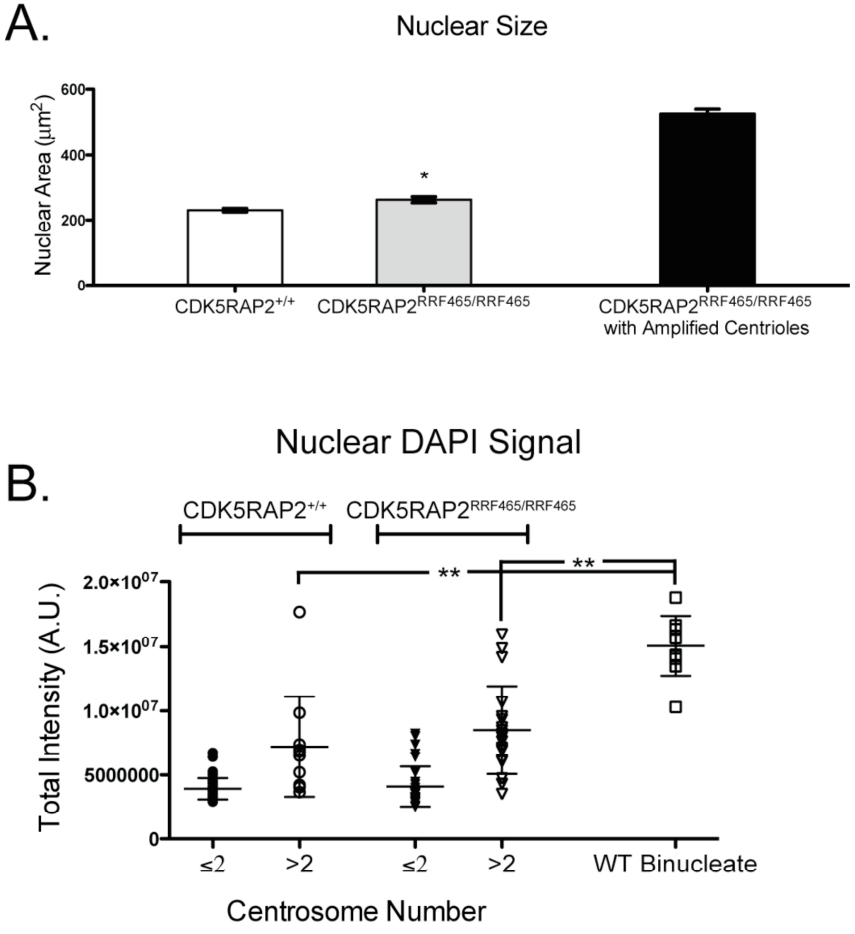


*Figure 2-10. CDK5RAP2$^{RRF465/RRF465}$ MEFs with amplified centrioles have enlarged nuclei*

(A) Nuclei are larger in *CDK5RAP2*$^{RRF465/RRF465}$ MEFs. Nuclei were stained with the DNA marker DAPI, and nuclear area ($\mu m^2$) was measured from micrographs (*CDK5RAP2*$^{+/+}$ : 230.3 $\mu m^2$ ± 5.6 $\mu m^2$ vs. *CDK5RAP2*$^{RRF465/RRF465}$: 262.0 $\mu m^2$ ± 9.5 $\mu m^2$, $p<0.05$); $n \geq 200$ cells per experiment. *CDK5RAP2*$^{RRF465/RRF465}$ MEFs with amplified centrioles predominate this phenotype, with an area of 528.0 $\mu m^2$ ± 13.4 $\mu m^2$; n = 50 cells per experiment. Data were collected from 3 independent experiments. (B) DAPI signal (arbitrary units) was quantified in *CDK5RAP2*$^{+/+}$ and *CDK5RAP2*$^{RRF465/RRF465}$ MEFs with one or two centrosomes (*CDK5RAP2*$^{+/+}$: 3.9 x $10^6$ ± 0.1x $10^6$, filled circle vs. *CDK5RAP2*$^{RRF465/RRF465}$: 4.0 x $10^6$ ± 0.3 x $10^6$, filled triangle) and MEFs with greater than two centrosomes (*CDK5RAP2*$^{+/+}$: 7.2 x $10^6$ ± 1.2 x $10^6$, $p<0.0001$, open circle vs. *CDK5RAP2*$^{RRF465/RRF465}$: 8.5 x $10^6$ ± 0.8 x $10^6$, $p<0.0001$, open triangle) and compared to wild-type binucleate cells (15.0 x $10^6$ ± 0.7 x $10^6$, open square); n = 10 and 11 for wild-type binucleates and *CDK5RAP2*$^{+/+}$ MEFs with one or two centrosomes, respectively and n = ≥20 for all other samples. There was no significant difference in DNA content between *CDK5RAP2*$^{+/+}$ and *CDK5RAP2*$^{RRF465/RRF465}$ MEFs whether they contained 1-2 or >2 centrosomes. Only binucleate cells showed a significant difference compared to the other groups. Error bars represent SEM.

Therefore, we conclude that *CDK5RAP2*$^{RRF465/RRF465}$ MEFs exhibit nuclear enlargement without increased DNA content, and that increased nuclear size correlates with centriole amplification.

### *CDK5RAP2 does not adversely affect the cell cycle*

In *CDK5RAP2*$^{RRF465/RRF465}$ MEFs centriole amplification could arise as an indirect effect on the cell cycle. Blocking of the cell cycle, specifically in S-phase, or failure of cytokinesis are possible causes of centriole amplification. To assess cell cycle block or delay, MEF cell cycle profiles were analyzed using flow cytometry. Cell cycle profiles from *CDK5RAP2*$^{+/+}$ and *CDK5RAP2*$^{RRF465/RRF465}$ cultures were indistinguishable (Figure 2-11A), indicating that centriole amplification in *CDK5RAP2*$^{RRF465/RRF465}$ MEFs is not due to an overt indirect effect on the cell cycle (Figure 2-11B). These data show that *CDK5RAP2*$^{RRF465/RRF465}$ MEFs have an altered centriole duplication cycle resulting in centriole amplification that is not due to indirect effects on the cell cycle.

### *Centrioles lose engagement and cohesion in CDK5RAP2 mutant MEFs*

In addition to centriole amplification, *CDK5RAP2*$^{RRF465/RRF465}$ MEFs showed a significantly higher incidence of single centrioles (Figure 2-7A and supplemental Table 2-2). This is in contrast to wild-type cells where centrioles are predominantly configured as pairs. Centriole configurations within MEFs were examined through immunofluorescence microscopy, using antibodies against the centriole marker, centrin and PCM marker γ-tubulin.

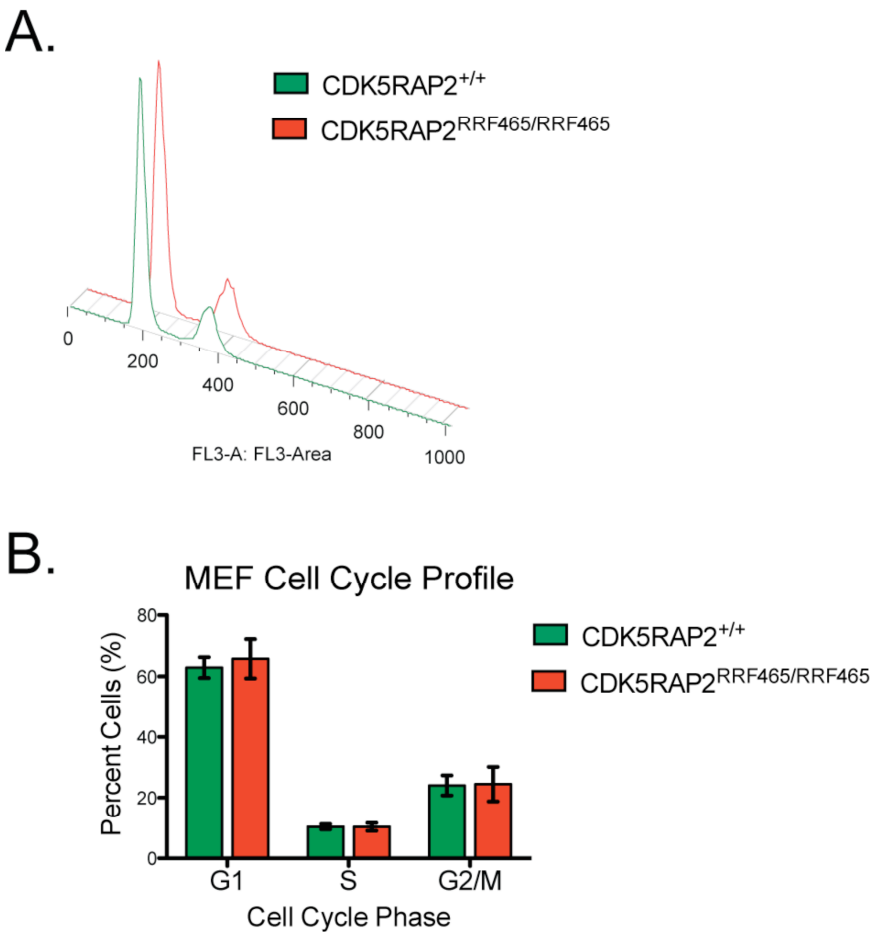


*Figure 2-11. Loss of CDK5RAP2 does not alter cell cycle progression*

(A) Cell cycle profiles of *CDK5RAP2*$^{+/+}$ and *CDK5RAP2*$^{RRF465/RRF465}$ MEF cultures (10,000 events were counted per genotype). Similar profiles were observed in three independent experiments.
(B) Quantification of the percent cells in G1 (*CDK5RAP2*$^{+/+}$: 62.9% ± 3.4% vs. *CDK5RAP2*$^{RRF465/RRF465}$: 65.8% ± 6.4%, p>0.05), S (*CDK5RAP2*$^{+/+}$: 10.4% ± 0.9% vs. *CDK5RAP2*$^{RRF465/RRF465}$: 10.3% ± 1.3%, p>0.05), or G2/M (*CDK5RAP2*$^{+/+}$: 24.1% ± 3.3% vs. *CDK5RAP2*$^{RRF465/RRF465}$: 24.5% ± 5.7%, p>0.05) stages of the cell cycle in *CDK5RAP2*$^{+/+}$ and *CDK5RAP2*$^{RRF465/RRF465}$ cultures. No significant differences between genotypes were observed. Data were collected from 3 independent experiments. Error bars represent SEM.

Typical of normal cells, *CDK5RAP2*$^{+/+}$ MEFs had two centrioles in close proximity that each assembled PCM in G1-phase, and two engaged pairs of centrioles, where each pair assembled PCM in G2-phase (2-7A). In contrast, *CDK5RAP2*$^{RRF465/RRF465}$ MEFs contained several different centriole configurations including paired centrioles, single centrioles and clusters of three or more centrioles (Figure 2-7A).

We further quantified these effects by counting mother and daughter centrioles immunostained for the mother centriole marker cenexin/ODF2 and γ-tubulin as a centriole marker. In this analysis, the paired configuration, including one mother and one daughter centriole, was used to describe "normal" centrosomes. The incidence of MEFs containing one or more singlet centrioles increased more than 4-fold in the *CDK5RAP2*$^{RRF465/RRF465}$ MEFs (40.8%) relative to *CDK5RAP2*$^{+/+}$ MEFs (9.7%) (Figure 2-12A) (Table 2-2 summarizes all centriole configurations). The presence of singlet centrioles indicates that both centriole engagement and cohesion failed. Normally, late in G2-phase, loss of centrosome cohesion occurs when centrosomes separate prior to mitotic spindle formation. A role for CDK5RAP2 in cohesion was previously reported by siRNA knockdown, yet no centriole amplification or disengagement was observed (Graser et al., 2007).

Another frequent centriole configuration seen in *CDK5RAP2*$^{RRF465/RRF465}$ MEFs was "daughter-daughter" pairs (Table 2-2). Centriole maturation, monitored by recruitment of cenexin/ODF2 to mother centrioles, occurs late in G2-phase (Lange and Gull, 1995). Therefore, the population of "daughter-daughter" centriole pairs, normally seen only in cells transiting between S- and G2-phase, will increase if centriole

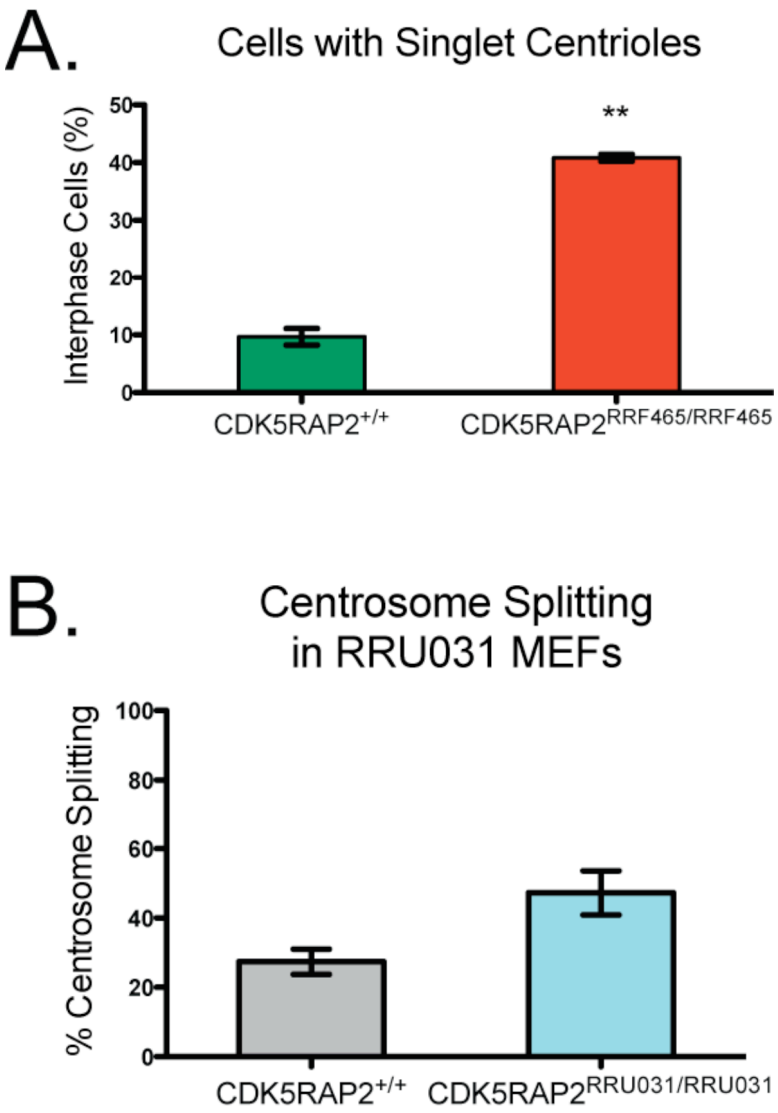


*Figure 2-12. CDK5RAP2 maintains centriole cohesion*

(A) Quantification of cells showing singlet centrioles in *CDK5RAP2*$^{+/+}$ (9.7% ± 1.4%, green bars) and *CDK5RAP2*$^{RRF465/RRF465}$ (40.8% ± 0.6%, $p<0.005$, red bars) cultures. Data were collected from 3 independent experiments, n = 200 cells per experiment.
(B) *CDK5RAP2*$^{RRU031/RRU031}$ MEFs had an increased incidence of centrosome splitting (*CDK5RAP2*$^{+/+}$: 27.4% ± 3.6% vs. *CDK5RAP2*$^{RRU031/RRU031}$: 47.2% ± 6.4%, $p<0.05$). Centrosome splitting was defined as centrosomes being >2μm apart. n = 110 cells total from five independent experiments. Error bars represent SEM.

| Table 2-2 Centriole Configurations | | | |
|---|---|---|---|
| | Key (● = mother centriole; ● = daughter centriole) | CDK5RAP2$^{+/+}$ | CDK5RAP2$^{RRF465/RRF465}$ |
| Paired (m/d) |  | 368 | 219 |
| 2 Singles (m/d) |  | 142 | 81 |
| 2 Pairs (m/d;m/d) |  | 8 | 33 |
| 2 Pairs Split (m/d;m/d) |  | 15 | 15 |
| 1 Pair (m/d) - 2 Singles (m/d) |  | 11 | 19 |
| 1 Pair (m/d) - 1 Single (m) |  | 1 | 15 |
| 1 Pair (m/d) - 1 Single (d) |  | 8 | 11 |
| 2 Pairs (m/d;d/d) |  | 2 | 3 |
| 2 Pairs Split (m/d;d/d) |  | 7 | 4 |
| 1 Pair (d/d) - 2 Singles (m/d) |  | 0 | 3 |
| 1 Pair (d/d) - 1 Single (m) |  | 0 | 2 |
| 1 Pair (d/d) - 1 Single (d) |  | 1 | 0 |
| 2 Pairs - All Singles (2m/2d) |  | 3 | 12 |
| 3 Singles (1 m) |  | 1 | 8 |
| 3 Singles (2 m) |  | 0 | 3 |
| >4 Singles |  | 1 | 10 |
| 1 Pair (m/d) - Overduplicated Singles |  | 5 | 23 |
| 1 Pair (d/d) - Overduplicated Singles |  | 4 | 4 |
| ≥2 Pairs ± Overduplicated Singles |  | 13 | 63 |
| 1 Triplet |  | 3 | 25 |
| 1 Triplet - Pair(s) |  | 1 | 11 |
| 1 Triplet - Single(s) |  | 4 | 14 |
| 1 Triplet - Pair(s) and Single(s) |  | 1 | 15 |
| 2 Triplets |  | 0 | 1 |
| 2 Triplets - Single(s) |  | 0 | 2 |
| 2 Triplets - Pair(s) and Single(s) |  | 0 | 4 |
| | | | |
| Cells with d/d Pairs | | 14 | 67 |

engagement fails and daughter centrioles re-duplicate. *CDK5RAP2*$^{RRF465/RRF465}$ MEFs showed an approximately 5-fold increase in daughter-daughter pairs (*CDK5RAP2*$^{+/+}$: 2.3% ± 0.4% vs. *CDK5RAP2*$^{RRF465/RRF465}$: 11.2% ± 1.2%, mean ± SEM, $p<0.05$) (Table 2-2). Thus, *CDK5RAP2*$^{RRF465/RRF465}$ centrioles lose engagement and become re-licensed to duplicate, as evidenced not only by the presence of singlet centrioles but also by the increased numbers of daughter-daughter pairs.

We reasoned that the low level of CDK5RAP2 expression in *CDK5RAP2*$^{RRU031/RRU031}$ MEFs might mimic siRNA knockdown. Therefore, we examined whether *CDK5RAP2*$^{RRU031/RRU031}$ MEFs also displayed loss of centriole cohesion. To test this idea immunofluorescence staining of PCM markers γ-tubulin and pericentrin was used to label centrosomes and to measure the intra-centrosomal distance. An intra-centrosomal distance larger than two microns is used as criterion to indicate that centrosomes are separated (Mayor et al., 2000). Indeed, we found that centrosome splitting increased by more than 70% in *CDK5RAP2*$^{RRU031/RRU031}$ MEFs compared to *CDK5RAP2*$^{+/+}$ *MEFs* (Figure 2-12B). These results show that *CDK5RAP2*$^{RRU031/RRU031}$ MEF centrioles lose cohesion prematurely. The fact that no singlet centrioles were observed in *CDK5RAP2*$^{RRU031/RRU031}$ MEFs indicated that premature loss of centriole cohesion was occurring within G2-phase We conclude that the RRU031 mutation is a weak loss of function *CDK5RAP2* mutation due to the low level expression of full-length CDK5RAP2. Moreover, we conclude that the hypomorphic phenotype of CDK5RAP2 is loss of centriole cohesion, whereas a strong loss of function results in loss of centriole cohesion and engagement.

*CDK5RAP2$^{RRF465/RRF465}$ MEFs assemble multipolar spindles*

The presence of supernumerary centrosomes is a potentially dangerous condition at mitosis because centrosomes are dominant MTOCs, and therefore have the potential to organize microtubules aberrantly in to the spindle apparatus and assemble multipolar spindles. A potential consequence of spindle multipolarity is the inappropriate segregation of chromosomes, which can lead to aneuploidy with increased cell death, but also a heightened propensity for tumorigenesis (Brinkley, 2001; Pihan and Doxsey, 2003; Nigg, 2006). Centrosome clustering at spindle poles assures spindle bipolarity in cells with more than two centrosomes (Quintyne et al., 2005; Basto et al., 2008; Kwon et al., 2008; Yang et al., 2008). Our definition of multipolar spindles required one or more MTOC(s) to be positioned more than 45º away from the major axis of the spindle, as determined from spindle microtubules and the configuration of aligned chromosomes (Figure 2-13A). We found that *CDK5RAP2$^{RRF465/RRF465}$* MEFs with two centrosomes formed bipolar spindles normally, as did *CDK5RAP2$^{+/+}$* MEFs. However, 51% of mitotic *CDK5RAP2$^{RRF465/RRF465}$* MEFs with supernumerary centrosomes formed multipolar spindles, while the remaining 49% assembled a bipolar, or pseudo-bipolar, spindle (Figure 2-13B). Since ~30% of *CDK5RAP2$^{RRF465/RRF465}$* had amplified centrioles, this amounts to approximately 15% of total mitotic *CDK5RAP2$^{RRF465/RRF465}$* MEFs that form multipolar spindles. Thus, centriole amplification in *CDK5RAP2$^{RRF465/RRF465}$* MEFs can lead to multipolar spindle formation. However, aberrant anaphase or telophase stage cells were not observed, an indication that multipolar spindles are resolved into pseudo-bipolar spindles before anaphase onset.

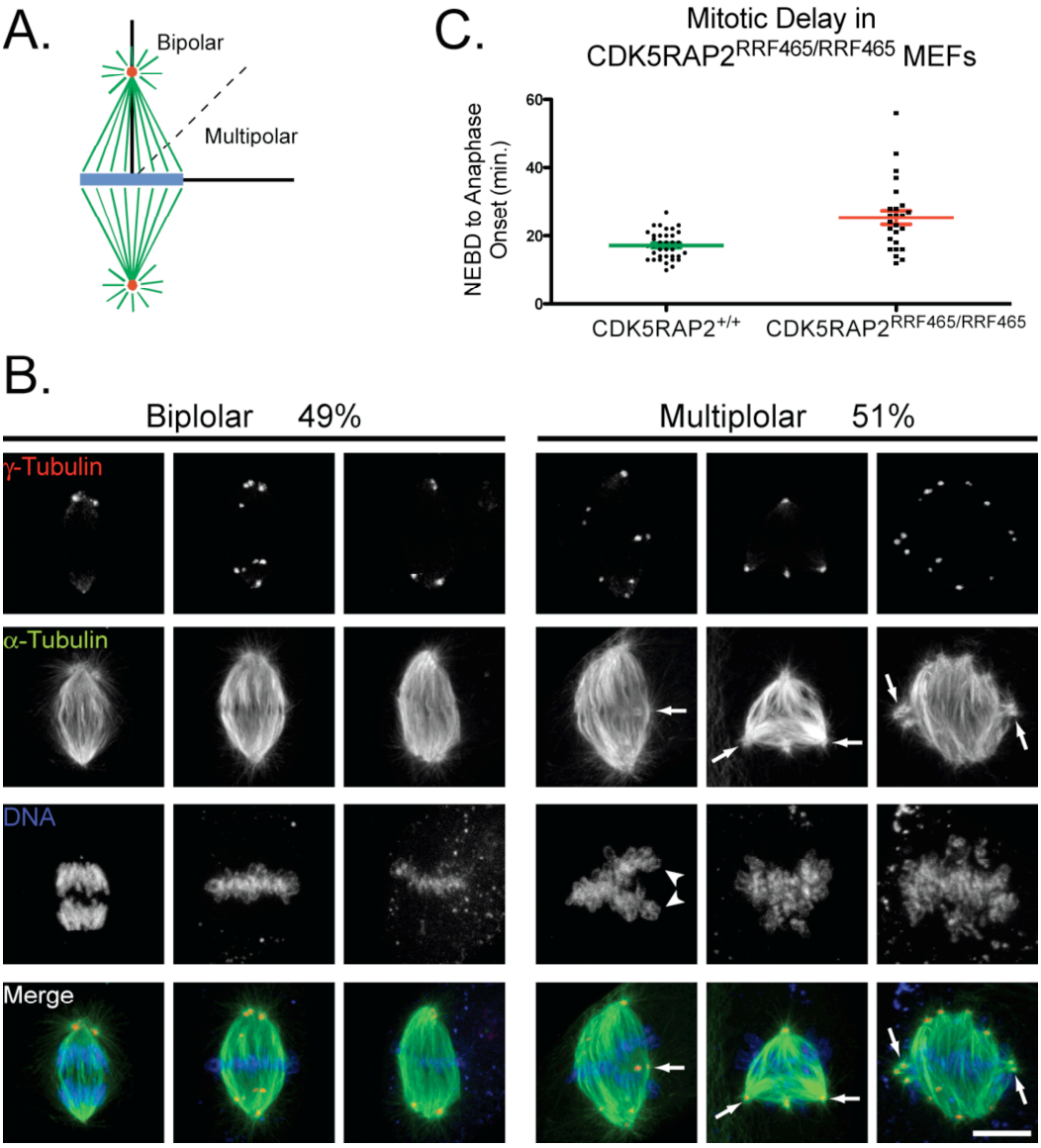


*Figure 2-13. Multipolar spindles form in CDK5RAP2$^{RRF465/RRF465}$ MEFs*

(A) Schematic outlining the criteria used to designate bipolar and multipolar spindles. To qualify as multipolar, spindles had to have an MTOC greater than 45º from the dominant spindle axis as determined from spindle microtubules and DNA alignment.
(B) Supernumerary centrosomes in *CDK5RAP2*$^{RRF465/RRF465}$ MEFs fail to cluster at mitosis, producing multipolar spindles. Immunofluorescence images of mitotic figures immunostained for γ-tubulin (1$^{st}$ row, red in merged panel), α-tubulin (2$^{nd}$ row, green in merge), and DNA (3$^{rd}$ row, blue in merge). In *CDK5RAP2*$^{RRF465/RRF465}$ mitotic MEFs with multiple centrosomes, 51% of mitotic spindles were multipolar (n = 43). Arrows indicate

examples of the excess spindle poles, and arrowheads indicate chromosomes configured improperly on the metaphase plate. Scale bar = 10 μm.
(C) Scatter plot showing the timing from nuclear envelope breakdown (NEBD) to anaphase onset in *CDK5RAP2*$^{+/+}$ and *CDK5RAP2*$^{RRF465/RRF465}$ MEFs. In a small population of *CDK5RAP2*$^{RRF465/RRF465}$ MEFs, the time between NEBD and anaphase onset was prolonged, with an approximately 8 min, or 47.7%, increase in the time spent to reach anaphase (*CDK5RAP2*$^{+/+}$: 17.2 min. ± 0.7 min. vs. *CDK5RAP2*$^{RRF465/RRF465}$: 25.4 min. ± 2.1 min., $p<0.0001$); $n \geq 25$. Error bars represent SEM.

Centrosome clustering is accomplished during a delay in mitosis due to activation of the spindle checkpoint by amplified centrosomes, allowing the cell time to correct spindle assembly defects (Basto et al., 2008; Kwon et al., 2008; Yang et al., 2008). Using live cell imaging, we observed an increase of approximately 48%, in the timing between nuclear envelope breakdown (NEBD) and anaphase onset in a population of *CDK5RAP2*$^{RRF465/RRF465}$ MEFs compared to *CDK5RAP2*$^{+/+}$ MEFs (Figure 2-13C). These results are consistent with the proposal that *CDK5RAP2*$^{RRF465/RRF465}$ MEFs accomplish spindle bipolarity by prolonging their stay in metaphase through activation of the spindle checkpoint, providing time for supernumerary centrosomes to cluster.

### *CDK5RAP2*$^{RRF465/RRF465}$ *MEFs have amplified mother centrioles and template multiple primary cilia*

New centrioles are form in S-phase and mature into mother centrioles in G2-phase of the succeeding cell cycle. Centriole amplification led us to hypothesize that *CDK5RAP2*$^{RRF465/RRF465}$ MEFs would have increased numbers of mother centrioles. To test this idea we used immunostaining for the mother centriole-specific protein cenexin/ODF2. We found that *CDK5RAP2*$^{RRF465/RRF465}$ MEFs possessed multiple mother centrioles and, since *CDK5RAP2*$^{RRF465/RRF465}$ MEFs exhibited no irregularities in cell cycle progression (Figure 2-11), we attributed this to the accumulation of mother centrioles following centriole amplification (Figure 2-14A). The majority of *CDK5RAP2*$^{+/+}$ MEFs contained one (89.3%) or two (8.2%) mother centrioles that paired with daughter centrioles, reflecting the G1/S- and G2-phases of the cell cycle,

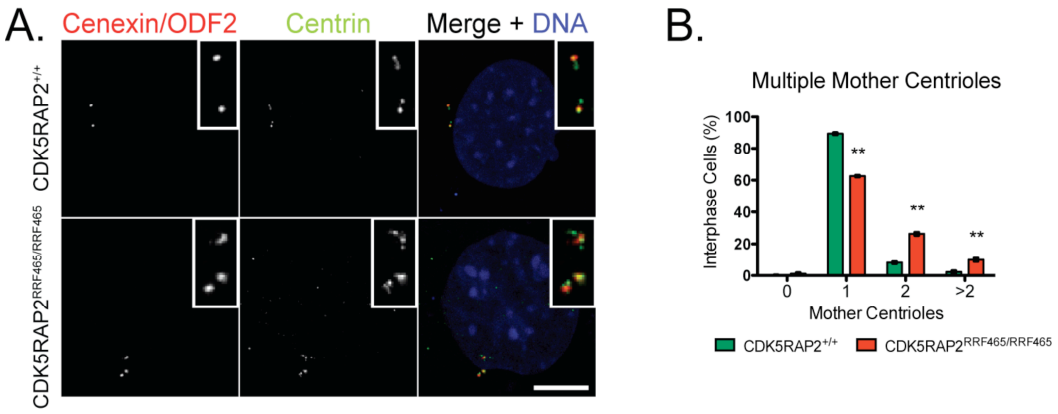


*Figure 2-14. CDK5RAP2$^{RRF465/RRF465}$ MEFs form multiple mother centrioles*

(A) Mother centrioles are amplified in *CDK5RAP2*$^{RRF465/RRF465}$ MEFs. Immunofluorescence images of *CDK5RAP2*$^{+/+}$ and *CDK5RAP2*$^{RRF465/RRF465}$ MEFs stained for the mother centriole marker cenexin/ODF2 (left, red in merged panel), centrin (middle, green in merged panel), and DNA (blue in merged panel). Insets are enlargements of the centrioles. Scale bar = 10 μm
(B) Percentages of cells with 0, 1, 2, or greater than 2 mother centrioles in *CDK5RAP2*$^{+/+}$ (green bars) and *CDK5RAP2*$^{RRF465/RRF465}$ (red bars) cells. MEFs containing 0 mother centrioles (*CDK5RAP2*$^{+/+}$: 0.2% ± 0.2% vs. *CDK5RAP2*$^{RRF465/RRF465}$: 1.2% vs. 0.7%, $p>0.05$), 1 mother centriole (*CDK5RAP2*$^{+/+}$: 89.3% ± 0.7% vs. *CDK5RAP2*$^{RRF465/RRF465}$: 62.5% ± 0.5%, $p<0.001$), 2 mother centrioles (*CDK5RAP2*$^{+/+}$: 8.2% ± 0.6% vs. *CDK5RAP2*$^{RRF465/RRF465}$: 26.3% ± 0.9%, $p<0.0005$), or more than 2 mother centrioles (*CDK5RAP2*$^{+/+}$: 2.3% ± 0.7% vs. *CDK5RAP2*$^{RRF465/RRF465}$: 10.0% ± 1.0%, $p<0.005$). Data were collected from three independent experiments, n = 200 cells per experiment. Error bars represent SEM.

respectively. In contrast, fewer *CDK5RAP2*$^{RRF465/RRF465}$ MEFs contained one mother centriole (62.5%), while significantly more cells contained two mother centrioles (26.3%). In addition, mother centriole numbers in excess of two were increased more than 4-fold in *CDK5RAP2*$^{RRF465/RRF465}$ MEFs (*CDK5RAP2*$^{+/+}$: 2.3% vs. *CDK5RAP2*$^{RRF465/RRF465}$: 10.0%) (Figure 2-14B). Since no affect on the cell cycle was observed, the increased number of *CDK5RAP2*$^{RRF465/RRF465}$ MEFs with two mother centrioles must represent a substantial fraction of cells in G1-phase with amplified mother centrioles. Taking this into consideration, we infer that approximately 28.1% of *CDK5RAP2*$^{RRF465/RRF465}$ MEFs have amplified mother centrioles.

Most vertebrate cells contain a single non-motile primary cilium. During G1-phase the mother centriole migrates to the plasma membrane and assumes the role of basal body and templates assembly of the primary cilium. We asked whether the amplification of mother centrioles in *CDK5RAP2*$^{RRF465/RRF465}$ MEFs was associated with changes in the proficiency and frequency of primary cilium assembly. When cultured in serum-deprived medium, many cells assemble a primary cilium upon entering G0, a prolonged resting state. We subjected MEFs to serum starvation and immunostained with antibodies directed at acetylated α-tubulin to label axoneme microtubules, and with γ-tubulin to label the centrioles/basal bodies (Figure 2-15A). *CDK5RAP2*$^{+/+}$ and *CDK5RAP2*$^{RRF465/RRF465}$ MEFs were equally proficient at primary cilium formation (*CDK5RAP2*$^{+/+}$: 71.2% vs. *CDK5RAP2*$^{RRF465/RRF465}$: 74.0%) (Figure 2-15B). *CDK5RAP2*$^{+/+}$ MEFs formed a single primary cilium templated from one of two interphase centrioles (Figure 2-15A,C). In contrast, *CDK5RAP2*$^{RRF465/RRF465}$ MEFs

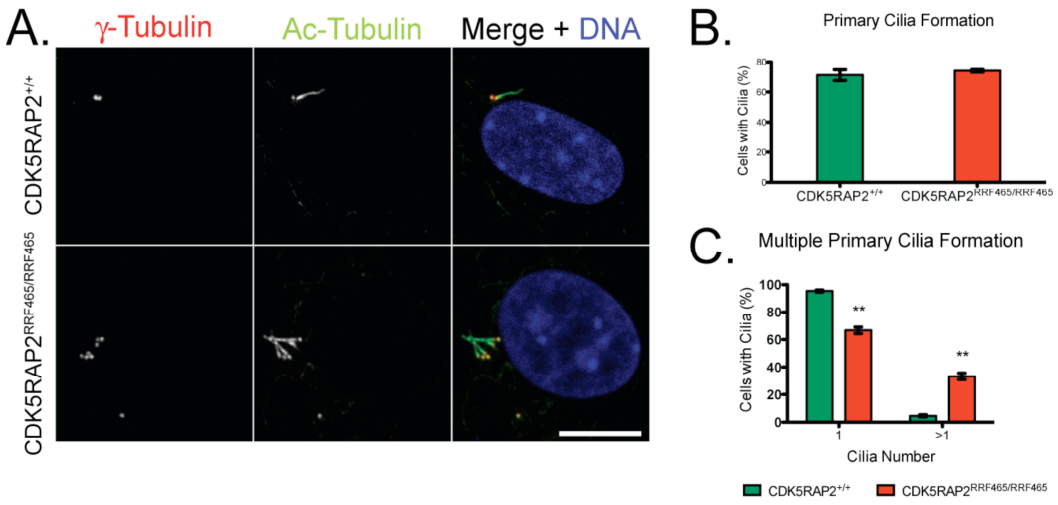


*Figure 2-15. CDK5RAP2$^{RRF465/RRF465}$ MEFs form multiple primary cilia*

(A) Extra centrioles in *CDK5RAP2*$^{RRF465/RRF465}$ MEFs template the formation of multiple primary cilia. Immunofluorescence images of *CDK5RAP2*$^{+/+}$ and *CDK5RAP2*$^{RRF465/RRF465}$ MEFs stained for γ-tubulin (left, red in merged panel), the cilium axoneme marker acetylated α-tubulin (middle, green in merged panel), and DNA (blue in merged panel). Scale bar = 10 μm.
(B) *CDK5RAP2*$^{+/+}$ and *CDK5RAP2*$^{RRF465/RRF465}$ MEFs are equally proficient at cilium formation. The graph shows the percent of cells that formed primary cilia in *CDK5RAP2*$^{+/+}$ (green bars) and *CDK5RAP2*$^{RRF465/RRF465}$ (red bars) MEFs (*CDK5RAP2*$^{+/+}$: 71.2% ± 3.6% vs. *CDK5RAP2*$^{RRF465/RRF465}$: 74.0% ± 0.9%, $p>0.05$). Data were collected from three independent experiments, n = 200 cells per experiment.
(C) A significantly greater number of *CDK5RAP2*$^{RRF465/RRF465}$ MEFs form multiple primary cilia. The graph shows the percent of MEFs forming a single primary cilium (*CDK5RAP2*$^{+/+}$: 95.3% ± 0.8% vs. *CDK5RAP2*$^{RRF465/RRF465}$: 66.7% ± 2.4%, $p<0.005$) or more than one primary cilium (*CDK5RAP2*$^{+/+}$, 4.7% ± 0.8% vs. *CDK5RAP2*$^{RRF465/RRF465}$, 33.3% ± 2.4%, $p<0.005$). Data were collected from three independent experiments, n = 150 cells with primary cilia per experiment. Error bars represent SEM.

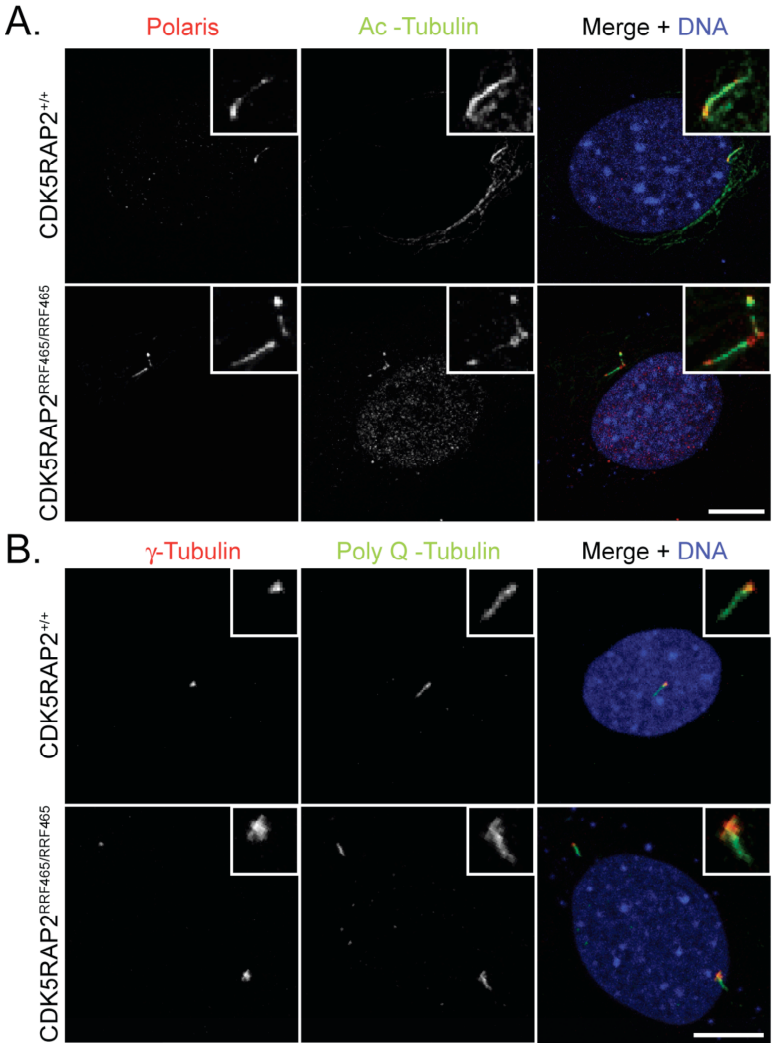


*Figure 2-16. Multiple primary cilia in CDK5RAP2$^{RRF465/RRF465}$ MEFs contain cilia transport proteins*

(A) Multiple primary cilia contain ciliary transport proteins. Immunofluorescence images of *CDK5RAP2*$^{+/+}$ and *CDK5RAP2*$^{RRF465/RRF465}$ MEFs stained for polaris/IFT88 (left, red in merged panel), γ-tubulin (middle, green in merged panel), and DNA (blue in merged panel). Insets show enlargements of the cilia regions.
(B) Excess centrioles in *CDK5RAP2*$^{RRF465/RRF465}$ MEFs template the formation of multiple primary cilia. Immunofluorescence images of *CDK5RAP2*$^{+/+}$ and *CDK5RAP2*$^{RRF465/RRF465}$ MEFs stained for γ-tubulin (left, red in merged panel), polyglutamylated-tubulin, another tubulin modification found on axonemal tubulin (middle, green in merged panel), and DNA (blue in merged panel). Scale bars = 10 μm.

showed a greater than 7-fold increase in formation of multiple primary cilia (*CDK5RAP2*$^{+/+}$: 4.7% vs. *CDK5RAP2*$^{RRF465/RRF465}$: 33.3%) (Figure 2-15C). This increase correlated well with the frequencies observed in centriole amplification (33%) (Figure 2-7B), and mother centriole amplification (28%) (Figure 2-14B). In order to confirm that the amplified microtubule based structures that we were observing with anti-acetylated tubulin staining were true primary cilia we immmunostained for poly-glutamylated tubulin (another tubulin modification commonly found in primary cilia) and polaris/IFT88 (an intra-flagellar transport protein) (Figure 2-16A,B). These data demonstrate that actively cycling mammalian cells can form more than one primary cilium if multiple mother centrioles are present.

### *CDK5RAP2 binds pericentrin*

A recent report showed that localization of CDK5RAP2 at centrosomes is inhibited by RNAi knockdown of the centrosomal protein pericentrin, however, CDK5RAP2 knockdown did not impact pericentrin localization (Graser et al., 2007). The dependence of CDK5RAP2 localization on pericentrin, along with the similarities in human diseases with mutations in these genes, led us to test for binding between CDK5RAP2 and pericentrin. We found that both isoforms of pericentrin, A and B, co-immunoprecipitated with CDK5RAP2 from NIH-3T3 fibroblasts (Figure 2-17A). However, the localization of pericentrin at the centrosome was similar in *CDK5RAP2*$^{+/+}$ and *CDK5RAP2*$^{RRF465/RRF465}$ MEFs (Figure 2-17B). These results suggest that the domain

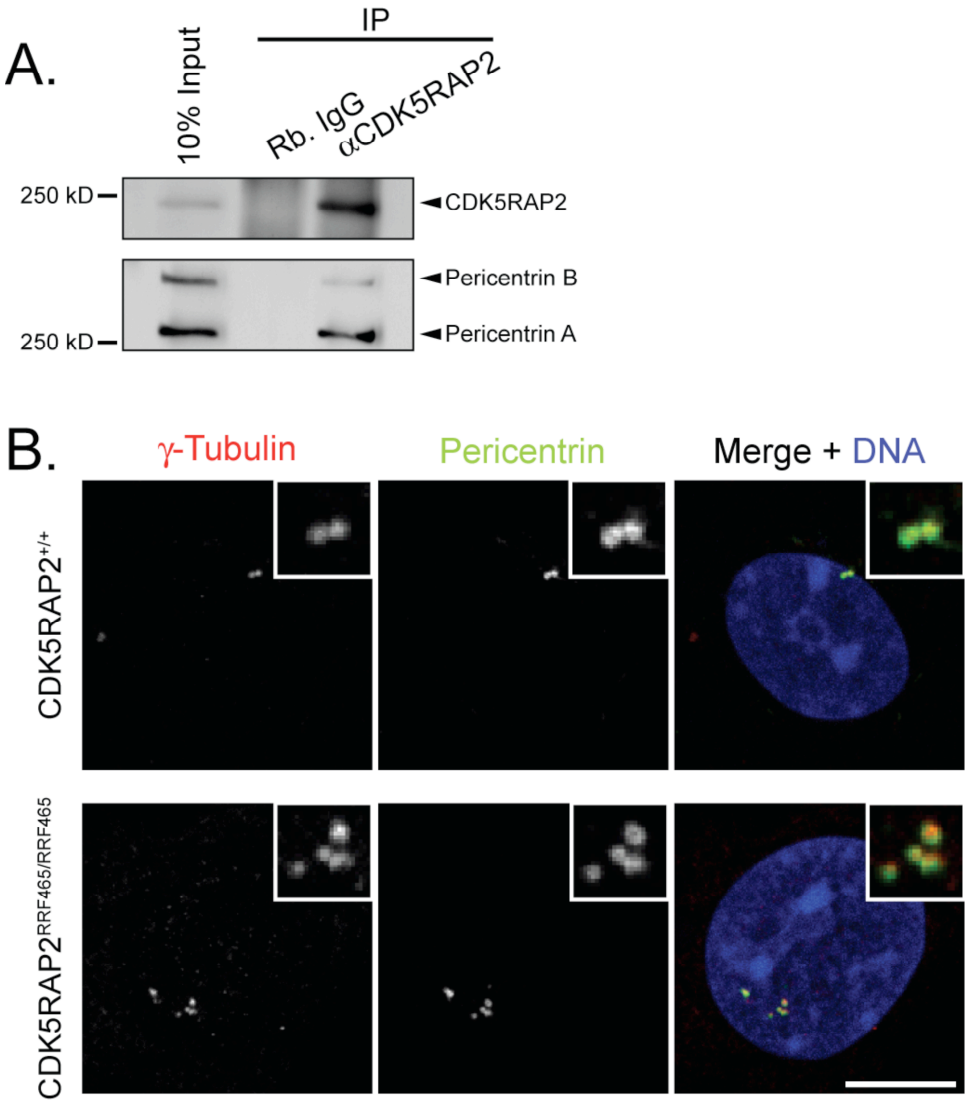


*Figure 2-17. CDK5RAP2 binds pericentrin*

(A) CDK5RAP2 binds pericentrin A and B in NIH-3T3 fibroblasts. Western blot of CDK5RAP2 immunoprecipitate from NIH-3T3 fibroblasts showed that CDK5RAP2 binds both pericentrin A and B. 10% input represents the lysate used for IP, and control rabbit IgG was used as a negative IP control.
(B) Pericentrin localization appears normal at *CDK5RAP2*$^{RRF465/RRF465}$ centrosomes. Immunofluorescence images of *CDK5RAP2*$^{+/+}$ and *CDK5RAP2*$^{RRF465/RRF465}$ MEFs stained for γ-tubulin (left, red in merged panel), pericentrin (middle, green in merged panel), and DNA (blue). Insets show enlargements of the centrosomes. Scale bar = 10 μm.

in CDK5RAP2 that binds to pericentrin may still be intact in the *CDK5RAP2*$^{RRF465/RRF465}$ truncation mutant.

**C. Conclusions**

Centrosomes are powerful MTOCs and therefore their numbers must be tightly regulated. In order to prevent centrosome amplification cells have developed mechanisms that restrict centriole duplication to occur only once per cell cycle. Furthermore, there are mechanisms that allow cells to cope with supernumerary centrosomes when they are present. Although recent research has begun to unravel the mysteries of such mechanisms much is still unknown. Our research has shown that CDK5RAP2 is important for maintaining centriole engagement and cohesion and our two distinct mutant lines have allowed us to uncover information as to the levels of CDK5RAP2 that are needed for these processes to fail. It will be important to see where CDK5RAP2 fits within the centriole engagement and cohesion pathways as more research uncovers other involved molecules.

Centriole numbers directly correlate with centrosome numbers and MTOCs. During mitosis, MTOCs nucleate spindle microtubules that form the bipolar spindle. The leading model for control of centriole duplication is maintenance of centriole engagement. That loss of CDK5RAP2 allows centriole amplification, shown here, is a novel finding that implicates its role in centriole engagement. MEFs derived from *CDK5RAP2* mutant mice exhibited centriole amplification. There was a 5-fold increase in MEFs with amplified centrioles.

Knockdown of CDK5RAP2 in mammalian cultured cells was previously reported to affect centrosome cohesion and γ-tubulin recruitment to centrosomes (Graser et al., 2007; Fong et al., 2008). We showed that one of our mutant lines (*CDK5RAP2*$^{RRU031/RRU031}$) is a hypomorph and also showed defects in centrosome cohesion, however they did not exhibit centriole amplification. *CDK5RAP2* mutant MEFs also showed defects in rootletin localization. Rootletin is a structural component of cohesion fibers and its loss has been shown to affect centriole cohesion (Bahe et al., 2005). The finding that 7% full-length CDK5RAP2 expression in our hypomorphic mutant is sufficient to rescue centriole duplication defects is astonishing and also speaks to the tight regulation of the cell over centriole duplication. That mutant MEFs did not displace γ-tubulin is in contradiction with the findings of Fong et al., however our mouse mutants carry mutations that result in protein truncations and therefore the interacting domain that may be needed to localize γ-tubulin may still be in tact. However, it is important to note that γ-tubulin displacement was also not observed by Graser et al.

Centriole amplification can also arise from indirect effects on the cell cycle. Therefore, it was important that we do experiments to test for cell cycle effects in our MEF cultures. We showed that the cell cycle in mutant and control MEFs were highly similar indicating that cell cycle blocks or cytokinesis defect were not the source of centriole amplification. Interestingly, we also found that centriole amplification did not halt the cell cycle. This was evident not only in flow cytometry data but also in the fact that mother centrioles were also amplified in *CDK5RAP2*$^{RRF465/RRF465}$ MEFs. Daughter centrioles take one and a half cell cycles to mature into mother centrioles. Taken together these results suggest that *CDK5RAP2*$^{RRF465/RRF465}$ MEFs progressed through mitosis with

amplified centrioles. In G1-phase, *CDK5RAP2*$^{RRF465/RRF465}$ MEFs form multiple primary cilia when amplified centrioles were present. Multiple primary cilia are sometimes found in highly specialized cells that have exited the cell cycle or transformed cancer cells, however primary cultured cells that are active in the cell cycle have a single primary cilium. It will be important to assess defects, if any, associated with forming multiple primary cilia.

The most direct defect attributed to centriole amplification that was observed in *CDK5RAP2*$^{RRF465/RRF465}$ MEFs was the formation of multipolar spindles. While they formed prior to anaphase we found no evidence to suggest that cell divided with multipolar spindles. Live cell imaging showed that, in line with published data (Quintyne et al., 2005; Basto et al., 2008; Kwon et al., 2008; Yang et al., 2008), *CDK5RAP2*$^{RRF465/RRF465}$ MEFs cluster amplified MTOCs into a pseudo-bipolar spindle prior to anaphase onset.

Another phenotype associated with complete loss of CDK5RAP2 was nuclear enlargement. Nuclear enlargement was observed to have a high correlation with centriole amplification suggesting that this phenotype may have direct links to the other phenotypes. Cell senescence and oncogenic cell transformations have been shown to increase nuclear size (Mocali et al., 2005; Tornoczky et al., 2007). In the case of cell senescence cells would exit the cell cycle and the cultures would not become confluent, while oncogenic transformation would cause rapid growth of cultured cells. We did observe that our *CDK5RAP2*$^{RRF465/RRF465}$ MEF cultures had to be seeded heavier that wild-type control cultures and although they would no longer grow to confluence the culture

did remain viable suggesting that cell senescence might have occurred prematurely. These data, however, are anecdotal and will have to be more rigorously tested.

## D. Materials and Methods

### *Plasmids and Antibodies*

The full length *mCDK5RAP2* entry cDNA clone was obtained from Kazuna DNA Research Institute (Nakajima et al., 2005) and was recombined into the pcDNA-DEST53 (Invitrogen) vector to produce the pcDNA-GFP-mCDK5RAP2 expression plasmid. The *CDK5RAP2* sequence corresponding to amino acids 24-278 was cloned into the pRSETB (Invitrogen) plasmid for expression in *E. coli* as a 6XHis-tagged fusion protein and purified by $Ni^{++}$-chelating Sepharose Fast Flow (Amersham Biosciences, Piscataway, NJ, USA) for antibody production. Polyclonal anti-CDK5RAP2 antisera were raised in rabbits by Cocalico Biological Inc. (Reamstown, PA, USA), and affinity-purified over a $CDK5RAP2^{24-278}$-coupled Affigel 10 column (Bio-Rad, Hercules, CA, USA). For immunostaining the following antibodies were used: rabbit anti-CDK5RAP2 1:5000, mouse anti-α-tubulin (DM1a) 1:1000 (Sigma, St. Louis, MO, USA), rabbit anti-γ-tubulin 1:500 (Sigma), mouse anti-acetylated α-tubulin (6-11B-1) 1:10000 (Sigma), mouse anti-polyglutamylated-tubulin (GT335) 1:1000 (from C. Janke, Centre National de la Recherche Scientifique, University Montpellier), rabbit anti-polaris 1:200 (from B. Yoder, University of Alabama at Birmingham), mouse anti-pericentrin (30) 1:500 (BD Biosciences, San Jose, CA, USA), mouse anti-green fluorescent protein 1:1000 (Invitrogen), human anti-rootletin 1:500 (Ab Serotec, Oxford, UK), mouse anti-centrin

(20H5) 1:1000 (from J. L. Salisbury, Mayo Clinic, Rochester, MN, USA), rabbit anti-cenexin/ODF2 1:150 (from K. Lee, National Cancer Institute, NIH, Bethesda, MD, USA), chicken anti-cenexin/ODF2 1:1000 (from E. Xu, Northwestern University, Chicago, IL, USA), rabbit anti-centrobin 1:100 (from K. Rhee, Seoul National University, Seoul, Korea). Secondary antibodies included: Alexa Fluor-488 and -546 coupled goat antibodies used at 1:400 (Molecular Probes, Eugene, OR, USA). Nuclear stains included DRAQ5 1:1000 (Axxora, San Diego, CA, USA) and DAPI 1 μg/ml (Molecular Probes). Antibodies used for Western blotting: anti-CDK5RAP2 1:5000, mouse anti-α-tubulin (DM1a) 1:1000 (Sigma), and mouse anti-pericentrin 1:1000 (BD Biosciences). HRP-conjugated anti-mouse and –rabbit secondary antibodies were diluted 1:20000 (Jackson ImmunoResearch Laboratories Inc., West Grove, PA, USA).

### *Mouse Genetics*

Chimeras were generated by injection of embryonic stem cells from clones RRF465 and RRU031 (Bay Genomics, San Francisco, CA, USA) into host C57BL/6J blastocysts and transferred into uteri of pseudo-pregnant C57BL/6J females. Male chimeras were mated with C57BL/6J females and F1 progeny were subsequently intercrossed. The β-Geo insertion site was mapped by Southern blotting and PCR analysis. Splice trap transposon sites were mapped to sites approximately 8.8 and 11.1 Kbp from the 5' ends of exons 3 and 12 in *CDK5RAP2*$^{RRU031}$ and *CDK5RAP2*$^{RRF465}$ mutant mouse lines respectively. Genotyping was done by PCR. Sequencing of these alleles revealed that, while the *CDK5RAP2*$^{RRF465}$ line had an intact transposon, the *CDK5RAP2*$^{RRU031}$ line had a 133 bp deletion at the 5' end of the transposon.

*MEF Derivation and culture*

Appearance of the copulatory plug (day E0.5) was used to stage embryos. MEFs were derived from gestation day E14.5 embryos from heterozygous mutant crosses. After removal of the head and internal organs, embryos were rinsed in phosphate-buffered saline (PBS) and incubated in 0.05% trypsin at 4ºC overnight in a sterile 10mL screw cap tube. Embryos were then mechanically dissociated with a 1ml pipette and allowed to settle. Cells from single embryos were plated onto a 100 mm culture dish (Grainer Bio-One, Frickenhausen, Germany) with DMEM containing 10% FBS, 100 U/ml penicillin and 100 μg/ml streptomycin and incubated at 37ºC in a 5% $CO_2$ and 5% $O_2$-humidified chamber. Cell culture reagents were purchased from GIBCO-BRL (Invitrogen, Carlsbad, CA, USA) except where noted. Plating after dissociation was considered passage 0 (P0) and the first replating 2 days later was P1. All experiments were performed using cells between passages P4 and P8, on sibling MEFs cultured side by side. MEF genotypes were confirmed by PCR.

*Cell Culture and Treatments*

NIH-3T3 cells were cultured in DMEM containing 10% FBS, 100 U/ml penicillin and 100 μg/ml streptomycin and incubated at 37ºC in a 5% $CO_2$-humidifier chamber. Cell culture reagents were purchased from GIBCO-BRL (Invitrogen, Carlsbad, CA, USA) except where noted. Serum starvation to induce cilium formation was accomplished by culturing cells in DMEM containing 0.5% FBS, 100 U/ml penicillin and

100 μg/ml streptomycin and incubated for 36 hours. Cells were cultured in complete media containing 30 μM Nocodazole (Sigma, St. Louis, MO, USA) for 2.5 hours to achieve microtubule depolymerization. MEFs were synchronized by double-thymidine block by incubating freshly plated cells for 12 hours in complete medium containing 2 mM thymidine (Sigma), released for 16 hours in complete medium, and then replated and incubated 12 hours in complete medium containing 2 mM thymidine. Cells were finally released for 8 hours before fixation to examine mitotic cells.

*Immunostaining and Microscopy*

Cells were seeded onto 4 well slides and incubated overnight. Next, cells were rinsed briefly (2 seconds) in PBS and fixed in -20ºC methanol for 10 minutes. After fixation cells were washed 5 min in PBS and primary antibodies added in staining solution (5 mg/ml BSA, 0.1% Saponin, and 0.1% Triton X-100) for 1 hour, thereafter cells were washed 3 times 5 min in PBS and secondary antibody conjugates to Alexa 488 or 546 (Invitrogen, Carlsbad, CA, USA) were applied at 1:500 dilution for 1 hour. Three 5 min washes in PBS preceded the mounting of slides. Cells were imaged with a Leica TCS SP2 confocal microscope (Leica, Wetzlar, Germany) with a 63X/NA1.4 oil immersion objective, or a Zeiss Axioskop microscope (Carl Zeiss, Inc., Oberkochen, Germany) with a 63X/NA1.4 oil immersion objective and a Coolsnap FX CCD camera (Photometrics, Tucson, AZ, USA) with Metamorph software (Molecular Devices, Downingtown, PA, USA). Where noted, imageJ (Rasband, W.S., ImageJ, U.S. National Institutes of Health, Bethesda, MD, USA) was used for data analysis.

*Tissue Sectioning and Microscopy*

A timed pregnant *CDK5RAP2*$^{+/RRF465}$ female that was mated with a heterozygous male was deeply anesthetized (12.5 mg/ml Tribromoethanol [Avertin], administered at 250 mg/kg, i.p.) followed by cervical dislocation. Embryonic brains were recovered, post-fixed overnight in 4% Paraformaldehyde in 0.1M phosphate buffer, cryoprotected in 30% sucrose in 0.1M phosphate buffer, and frozen in -80°C 2-methylbutane. Frozen 30-μm thick sections were immunostained on-slide. The tissue was incubated in primary antibodies overnight, washed, and then incubated with secondary antibodies for two hours. Sections were imaged as described above. For adult brain sections, *CDK5RAP2*$^{+/+}$ and *CDK5RAP2*$^{RRF465/RRF465}$ mice and brains were processed as above, fixed overnight in 4% Paraformaldehyde in PBS and embedded in paraffin. Mounted 20μm thick coronal sections were stained 1 minute in Harris Hematoxylin (American Master Tech Inc., Lodi, CA, USA), washed 1 minute in water, rinsed in Scott's Solution, stained 1 minute in Eosin Y stain (American Master Tech Inc.), and dehydrated in ethanol (95% followed by 100% ethanol), quickly rinsed in Xylene and coverslip mounted with Permount (Fisher Scientific, Fairlawn, NJ, USA).

*Immunoblotting and Immunoprecipitation*

Whole cell lysates for immunoblotting were prepared by heating cells 5 min at 95ºC in 2X SDS-PAGE loading buffer (117 mM Tris-HCl pH 6.8, 10% glycerol, 3% SDS, 2% β-mercaptoethanol and 0.2% bromophenol blue). Whole cell lysates for immunoprecipitations were prepared by lysing cells 30 min. at 4ºC on a rotator in

Nonidet-P40 (NP40) lysis buffer (20 mM Tris-HCl pH 8.0, 137 mM NaCl, 10% glycerol, 1% NP40 and 2 mM EDTA) supplemented with 2 μg/ml Aprotinin, 10 mM NaF, 1X protease inhibitor cocktail (Sigma), 1 mM orthovanadate, 1 mM PMSF, 0.1 mM benzamidine-HCl, and 1 μg/ml phenanthroline. Whole cell lysates were separated by 6% SDS PAGE gel electrophoresis followed by immunoblotting and detection with HRP-conjugated secondary antibodies and the enhanced SuperSignal West Pico Chemiluminescent Substrate (Pierce, Rockford, IL, USA).

Immunoprecipitations were performed using 2 mg of whole cell lysate in NP40 lysis buffer + 2 μg of the indicated antibody + 10 μM Colcemid (Axxora) on a rotator at 4ºC overnight. The antibody/lysate mix was then incubated with pre-equilibrated Protein A Sepharose (Amersham Biosciences) for 4 hours at 4ºC. After centrifugation, the slurry was washed 3 times with ice-cold NP40 lysis buffer and proteins were eluted with 2X SDS-PAGE loading buffer.

*Flow Cytometry*

MEF cell cycle analysis was accomplished by propidium iodide (PI) (Invitrogen) staining of DNA and flow cytometry as described in *Current Protocols in Cytometry* (2008). In brief, cells were washed in PBS and fixed in 70% ice-cold ethanol. Ethanol was removed and cells were resuspended to a final concentration ~$10^6$ $ml^{-1}$ in staining solution (20 μg/ml PI, 200 μg/ml RNaseA, 0.1% Triton-X-100). Fluorescence was measured (Becton Dickinson, FACScan) for 10,000 cells per sample, and the data analyzed with FlowJo 8.8 software (Tree Star Inc, Ashland, OR) using a Watson Pragmatic fitting algorithm.

*Live Cell Imaging*

Time-lapse Differential Interference Contrast (DIC) microscopy was performed in Joachim Seemann's lab in the Department of Cell Biology, UT Southwestern Medical Center, cells grown for two days on 35 mm glass bottom culture dishes (MatTek, Ashland, MA, USA) were imaged in $CO_2$-Independent Medium supplemented with 2 mM L-alanyl-L-glutamine, 100 U/ml streptomycin, 100 mg/ml penicillin (Invitrogen) and 10% FCS (Invitrogen). Temperature was maintained using an XL-3 stage incubator (Carl Zeiss, Inc.) set at 37°C. DIC images were collected every minute for 12 hours on an Axiovert 200M microscope (Carl Zeiss, Inc.) with an Achroplan 10x/0.25 objective (Carl Zeiss, Inc.) and an Orca-285 camera (Hamamatsu Photonics, Hamamatsu City, Japan) in combination with the software package Openlab 4.02 (PerkinElmer, Waltham, MD, USA). Data were subsequently analyzed using ImageJ (NIH, Bethesda, MD).

*Statistical Analysis*

Statistical analyses were performed using Prism 5 (GraphPad Software, Inc., San Diego, CA). All statistical tests were two-tailed (unpaired Student's t-test) and were considered to be statistically significant at $p<0.05$. An * denotes $p<0.05$ and ** denotes $p<0.01$.

# CHAPTER THREE

# CONCLUSIONS AND FUTURE DIRECTIONS

Our data show that CDK5RAP2 maintains centriole engagement and cohesion. Since centriole disengagement is the licensing step that initiates centriole replication (Tsou and Stearns, 2006b, a; Nigg, 2007), the loss of CDK5RAP2 activity results in centriole amplification due to the failure to maintain engagement of mother-daughter pairs. CDK5RAP2 is therefore the first negative regulator of centriole licensing. The amplified centrioles in *CDK5RAP2*$^{RRF465/RRF465}$ MEFs impact not only mitotic spindle assembly but also promote assembly of multiple primary cilia, templated by the excess centrioles that accumulate in these cells.

## *CDK5RAP2's role in centriole engagement and cohesion*

The presence of single centrioles is an uncommon occurrence in wild-type cells because mother-daughter centriole pairs remain engaged following duplication until anaphase (Tsou and Stearns, 2006b, a; Nigg, 2007). Following disengagement, the centriole pair normally remains in close proximity through cohesion, which persists from G1-phase through the G2-/M-phase transition. The scattering of singlet centrioles and the centriole amplification in *CDK5RAP2*$^{RRF465/RRF465}$ MEFs show that engagement and cohesion both require CDK5RAP2 function. Moreover, from the two mutants we have generated, one hypomorphic and one strong, it is evident that centrosome cohesion is more sensitive to disruption of CDK5RAP2 than is engagement. Thus, even the low

(approximately 7% of endogenous) level of CDK5RAP2 expression from the leaky allele was sufficient to maintain centriole engagement.

The prevailing model for control of centriole replication underscores disengagement as the initiating step for centriole licensing: the step in the cell cycle that authorizes a single round of centriole replication (Tsou and Stearns, 2006b, a; Nigg, 2007). Disengagement is activated by separase at the metaphase-to-anaphase transition (Tsou and Stearns, 2006b). The molecules required to maintain engagement of centrioles, thus preventing re-licensing and restricting duplication, are not known. Our data indicate that CDK5RAP2 is required to restrict centriole duplication by maintaining mother-daughter centrioles in the engaged state. The prevalence of singlet centrioles and excess daughter-daughter pairs strongly implicates premature disengagement combined with re-licensing as mechanisms underlying centriole amplification in *CDK5RAP2*$^{RRF465/RRF465}$ MEFs.

Since separase initiates disengagement, it is possible that CDK5RAP2 is a target of this protease or that its localization or activity is inhibited by separase. We tested CDK5RAP2 as a separase substrate using *in vitro* translated human CDK5RAP2 with purified human separase, but detected no apparent cleavage of CDK5RAP2 (data not shown). Despite this negative result we cannot rule out the possibility that additional factors, post-translational modifications, or its centriolar context are needed for separase to target CDK5RAP2. The extent of the relationship between these two engagement regulators remains to be determined.

An alternative hypothesis for the amplification of centrioles in *CDK5RAP2*$^{RRF465/RRF465}$ MEFs is unrestricted *de novo* centriole biogenesis. In contrast to

the canonical "templated" assembly of daughters from mothers, centrioles can form in cells that lack any centrioles by *de novo* assembly (Marshall et al., 2001; Khodjakov et al., 2002; La Terra et al., 2005; Uetake et al., 2007). However, the presence of even one centriole in a cell suppresses *de novo* centriole assembly (La Terra et al., 2005). Since centrioles are present in *CDK5RAP2*$^{RRF465/RRF465}$ MEFs during amplification we favor the loss of engagement/re-licensing model as proposed above. However, we cannot exclude the possibility that CDK5RAP2 suppresses *de novo* centriole formation.

How CDK5RAP2 regulates engagement and cohesion is unclear, but it is likely that these two centriole-binding processes are related at the molecular level, as demonstrated by the *CDK5RAP2* mutant phenotypes. The displacement of rootletin, a structural component of cohesion fibers (Bahe et al., 2005), from its normal localization pattern at *CDK5RAP2* mutant centrosomes is consistent with the role for CDK5RAP2 in maintaining cohesion, as presented here and reported recently by RNAi knockdown in cell culture (Graser et al., 2007). That the RNAi depletion of CDK5RAP2 did not produce the single centrioles and centriole amplification phenotypes reported here is likely due to the partial depletion of CDK5RAP2 by siRNAs. This supposition is strongly supported by our results with the weak *CDK5RAP2* mutation in *CDK5RAP2*$^{RRU031/RRU031}$ MEFs where singlet centrioles were also not observed showing that centriole cohesion is prematurely lost after S-phase. Thus, partial loss of CDK5RAP2 function results in loss of cohesion, while strong loss of function additionally results in loss of engagement.

Another recent study, again targeting CDK5RAP2 by RNAi, reported that depletion of CDK5RAP2 disrupted mitotic centrosome MTOC activity and γ-tubulin recruitment (Fong et al., 2008), similar to the phenotype of *cnn* mutant Drosophila cells

(Megraw et al., 2001). In contrast, we observed no apparent effect on mitotic centrosome MTOC activity or γ-tubulin recruitment to centrosomes in *CDK5RAP2*$^{RRF465/RRF465}$ MEFs. Nevertheless, the possibility remains that such a function is retained by the first 435 amino acids of CDK5RAP2, which are still present in our truncation mutant. It is also possible that off-target affects contributed to the phenotypes seen by Fong *et al*. Myomegalin/ PDE4DIP, the other centrosomin ortholog in mammals (Verde et al., 2001), might work redundantly with CDK5RAP2 in mitotic centrosome assembly and could have been an off-target in those experiments. Since antibodies against mouse myomegalin were unavailable, we were unable to examine its expression or the effect, if any, of *CDK5RAP2* mutations on myomegalin localization. It remains possible that myomegalin shares redundant functions with CDK5RAP2 in mitotic centrosome function, similar to the defined role for centrosomin in Drosophila.

### *Mitotic function of CDK5RAP2*

Centrosome clustering is an important mechanism to prevent cells with amplified centrosomes from assembling multipolar mitotic spindles and contributing to genomic instability (Brinkley, 2001). Recent studies have shown that efficient centrosome clustering at mitosis requires cytoplasmic dynein (Quintyne et al., 2005) and Ncd, a kinesin-14 motor protein (Basto et al., 2008; Kwon et al., 2008), along with a host of other factors identified in a recent screen in Drosophila (Kwon et al., 2008). Interestingly, the presence of multipolar spindles, and not multiple centrosomes *per se*, activates the spindle assembly checkpoint, allowing time for excess centrosomes to cluster into two poles (Sluder et al., 1997; Basto et al., 2008; Kwon et al., 2008; Yang et al., 2008).

At mitosis, extra centrosomes in *CDK5RAP2*$^{RRF465/RRF465}$ MEFs are functional MTOCs, and behave as dominant organizers of spindle poles. Strikingly, 51% of mitotic *CDK5RAP2*$^{RRF465/RRF465}$ MEFs with amplified centrioles displayed multipolar spindles. However, the lack of altered anaphase or telophase stage cells indicates that these cells resolve the multipolar spindles. Consistent with this, live cell analysis showed that a small population *CDK5RAP2*$^{RRF465/RRF465}$ MEFs were delayed between nuclear envelope breakdown and anaphase onset, likely due to checkpoint activation in cells with amplified centrosomes.

Although the centrosome clustering mechanism is used to maintain genomic stability during cell division, it is currently unknown how multiple centrosomes affect asymmetric cell division, a complex type of cell division that requires alignment of the mitotic spindle relative to cortical determinants. It remains possible that pseudo-bipolar spindles are unable to properly align during asymmetric cell division.

### *Consequences of CDK5RAP2 loss of function on cell proliferation*

After a limited number of cell divisions, cultured diploid fibroblasts undergo cell cycle arrest and become senescent (Hayflick and Moorhead, 1961); these cells assume a large flat morphology and develop larger nuclei due to accumulation of DNA damage (Mocali et al., 2005). Two conditions have been shown to induce cell senescence: telomere shortening and genetic insults that result in activation of oncogenic products (Allsopp et al., 1995; Serrano et al., 1997).

Here we show that *CDK5RAP2*$^{RRF465/RRF465}$ MEFs had large nuclei that were associated with centriole amplification. We observed differences in the growth capacities

of sibling MEFs cultured side by side. Whereas *CDK5RAP2*$^{+/+}$ MEFs proliferated to passage 15 (P15), in contrast, *CDK5RAP2*$^{RRF465/RRF465}$ MEF proliferations slowed or arrested between P8 and P10, and after P4 a higher percent of cells were needed to seed a culture. Following P8-P10, *CDK5RAP2*$^{RRF465/RRF465}$ MEFs remained viable but would no longer grow to confluence. The underlying cause of this premature senescence and its link to centriole amplification is unclear. However, mutations in *pericentrin* lead to defects in ATR-dependent checkpoint signaling, revealing a molecular link between pericentrin, centrosome function and DNA repair (Griffith et al., 2008). Similarly, since CDK5RAP2 associates with pericentrin, *CDK5RAP2*$^{RRF465/RRF465}$ cells may also accumulate DNA lesions that limit their replicative potential. The culmination of these events may explain the limited proliferation capacity of *CDK5RAP2*$^{RRF465/RRF465}$ MEFs and suggests that *CDK5RAP2*$^{RRF465/RRF465}$ mice may be predisposed to cancer. We did not, however, observe a reduced lifespan for *CDK5RAP2* mutant mice nor an increase in visible tumors in our preliminary examinations.

### *Primary cilium assembly*

The primary cilium, once thought to be a cell vestige with no function, has emerged recently as a key signaling "antenna" for the cell (Singla and Reiter, 2006). While some differentiated cells have abundant motile cilia (Vladar and Stearns, 2007), and even some cancer cell lines exhibit multiple cilia of the motile class (Reilova-Velez and Seiler, 1984; van Haaften-Day et al., 1992; Vladar and Stearns, 2007), to our knowledge this is the first report of a high incidence of multiple primary cilia in a primary cell line. Cilia are essential contributors to cell signaling and it will be important

to determine the impact of multiple primary cilia on signaling levels and its potential effects on the *CDK5RAP2* disease pathology in humans. Increased cell signaling also holds the potential to cause enlarged nuclei as is cancer cells (Tornoczky et al., 2007) and therefore this may be the underlying cause for large nuclei forming in cells with amplified centrioles.

### *CDK5RAP2 mutant mice*

Our characterization of the *CDK5RAP2* mutant mice has not revealed any overt defects in somatic growth, body weight, adult behavior, or female fertility. Male fertility was mixed, with about 33% of males showing reduced fertility in $CDK5RAP2^{RRF465/RRF465}$ mice. Male infertility might be a genetic background effect, a possibility that will be tested via backcrosses to the C57BL/6 and 129Ola strains. Brain size and gross morphology appeared to be normal, indicating that disruption of CDK5RAP2 does not cause microcephaly in mice. It is possible that in mice, unlike in humans, the development of the cerebral cortex is not *CDK5RAP2*-dependent. In one scenario, mice may have redundancy in CDK5RAP2 function, and compensatory mechanism(s) might account for the lack of an obvious brain phenotype in this mutant. Myomegalin might play this role. Alternatively, CDK5RAP2 may be required in humans to populate the cerebral cortex with the significantly larger number of neurons ($10^{11}$) than exist in the mouse ($10^{7}$), and was proposed to involve an extra set of neural progenitors (Fish et al., 2008).

The physiological consequences of the plethora of cellular defects we describe, including multiple centrosomes in interphase and mitotic cells, and excess numbers of

primary cilia in *CDK5RAP2*$^{RRF465/RRF465}$ mice are at present unknown. The centrosome amplification observed in *CDK5RAP2*$^{RRF465/RRF465}$ fetal brain tissue suggests that this may be linked to the etiology of human MCPH. Moreover, the establishment of this mouse mutant will enable deeper investigations into the mechanisms by which the organism "copes" with these centrosome-based aberrations during development and in the adult. Nevertheless, the etiological basis for defective centrosomes leading to autosomal recessive primary microcephaly in humans remains to be elucidated. One possible mechanism might be a primary defect in neural stem cell divisions caused by the presence of multipolar spindles. Early in the development of the cerebral cortex, ventricular neural stem cells divide symmetrically to expand the progenitor pool; neurons arise somewhat later from asymmetric cell divisions of ventricular stem cells and from symmetric divisions of intermediate cortical progenitor cells (Fish et al., 2006; Buchman and Tsai, 2007; Fish et al., 2008). Populating the developing brain is a game of numbers. Ventricular neural stem cells must divide not only to expand and maintain the stem cell pool but also to produce differentiated brain cells. Therefore, a modest (approximately 30%) defect, such as the centriole amplification presented here, can end up having adverse effects on the overall development process. Defects that lead to ventricular neural stem cell loss will not only eliminate the stem cell but also all potential differentiated cells that would have been derived from that stem cell. However, since the mouse cerebral cortex is relatively small compared to primates, perhaps the necessity of attaining or maintaining peak progenitor numbers is not as stringently required in this species. Alternatively, other differences in cerebral cortex development between mouse and human may account for the different requirements for CDK5RAP2.

In summary, we report that CDK5RAP2 is a negative regulator of centriole replication that maintains centriole engagement and cohesion. We propose that the loss of engaged centrioles, but not the loss of cohesion, in *CDK5RAP2* mutant cells permits the repeated duplication of daughter centrioles. The consequences of centriole amplification in the *CDK5RAP2*$^{RRF465/RRF465}$ mutant are the assembly of multipolar mitotic spindles and excess primary cilia. The disruption of one or more of these centrosome functions in humans with homozygous mutations in *CDK5RAP2* is likely the etiological basis for the clinical manifestations associated with MCPH. The *CDK5RAP2* mutant mouse models presented here will be useful in understanding the regulation of centriole duplication, the importance of centriole cohesion, and the impact that disruption of these processes may have on MCPH.

**ACKNOWLEDGEMENTS**

I sincerely thank my mentor, Timothy L. Megraw, for his scientific guidance and for fostering my scientific maturity for the past five years. I would also like to thank the other members of the Megraw lab; Ling-Rong Kao, Jiuli Zhang, Raymond Jones, Violane Mottier and Shaila Kotadia for all of the helpful discussions and for sharing in the excitement of the experimental data. I will be forever be indebted to our collaborators; Robert (Bob) Hammer and Sarah Comerford derived the mutant mouse lines that were used in these studies. They have also played a great role in my scientific maturation process and for that I am truly grateful. Jannon Fuchs assisted us with the in vivo aspects of our project. Joachim Seemann was extremely instrumental in performing the DIC live cell imaging experiments. Lastly, I thank my committee, Timothy L. Megraw, Robert (Bob) Hammer, William (Bill) Snell, and Hui Zou for overseeing and guiding my graduate studies.

## BIBLIOGRAPHY


Allsopp, R.C., Chang, E., Kashefi-Aazam, M., Rogaev, E.I., Piatyszek, M.A., Shay, J.W., and Harley, C.B. (1995). Telomere shortening is associated with cell division in vitro and in vivo. Exp Cell Res *220*, 194-200.

Azimzadeh, J., and Bornens, M. (2007). Structure and duplication of the centrosome. J Cell Sci *120*, 2139-2142.

Bahe, S., Stierhof, Y.D., Wilkinson, C.J., Leiss, F., and Nigg, E.A. (2005). Rootletin forms centriole-associated filaments and functions in centrosome cohesion. J Cell Biol *171*, 27-33.

Basto, R., Brunk, K., Vinadogrova, T., Peel, N., Franz, A., Khodjakov, A., and Raff, J.W. (2008). Centrosome amplification can initiate tumorigenesis in flies. Cell *133*, 1032-1042.

Bettencourt-Dias, M., and Glover, D.M. (2007). Centrosome biogenesis and function: centrosomics brings new understanding. Nat Rev Mol Cell Biol *8*, 451-463.

Bobinnec, Y., Khodjakov, A., Mir, L.M., Rieder, C.L., Edde, B., and Bornens, M. (1998). Centriole disassembly in vivo and its effect on centrosome structure and function in vertebrate cells. J Cell Biol *143*, 1575-1589.

Bond, J., Roberts, E., Mochida, G.H., Hampshire, D.J., Scott, S., Askham, J.M., Springell, K., Mahadevan, M., Crow, Y.J., Markham, A.F.*, et al.* (2002). ASPM is a major determinant of cerebral cortical size. Nat Genet *32*, 316-320.

Bond, J., Roberts, E., Springell, K., Lizarraga, S.B., Scott, S., Higgins, J., Hampshire, D.J., Morrison, E.E., Leal, G.F., Silva, E.O., *et al.* (2005). A centrosomal mechanism involving CDK5RAP2 and CENPJ controls brain size. Nat Genet *37*, 353-355.

Bond, J., and Woods, C.G. (2006). Cytoskeletal genes regulating brain size. Curr Opin Cell Biol *18*, 95-101.

Bornens, M. (2002). Centrosome composition and microtubule anchoring mechanisms. Curr Opin Cell Biol *14*, 25-34.

Brinkley, B.R. (2001). Managing the centrosome numbers game: from chaos to stability in cancer cell division. Trends Cell Biol *11*, 18-21.

Buchman, J.J., and Tsai, L.H. (2007). Spindle regulation in neural precursors of flies and mammals. Nature reviews *8*, 89-100.

Caviness, V.S., Jr., Takahashi, T., and Nowakowski, R.S. (1995). Numbers, time and neocortical neuronogenesis: a general developmental and evolutionary model. Trends Neurosci *18*, 379-383.

Ching, Y.P., Qi, Z., and Wang, J.H. (2000). Cloning of three novel neuronal Cdk5 activator binding proteins. Gene *242*, 285-294.

Cowie, V. (1960). The genetics and sub-classification of microcephaly. J Ment Defic Res *4*, 42-47.

Delattre, M., Leidel, S., Wani, K., Baumer, K., Bamat, J., Schnabel, H., Feichtinger, R., Schnabel, R., and Gonczy, P. (2004). Centriolar SAS-5 is required for centrosome duplication in C. elegans. Nat Cell Biol *6*, 656-664.

Doxsey, S.J. (2001). Centrosomes as command centres for cellular control. Nat Cell Biol *3*, E105-108.

Faragher, A.J., and Fry, A.M. (2003). Nek2A kinase stimulates centrosome disjunction and is required for formation of bipolar mitotic spindles. Mol Biol Cell *14*, 2876-2889.

Fish, J.L., Dehay, C., Kennedy, H., and Huttner, W.B. (2008). Making bigger brains-the evolution of neural-progenitor-cell division. J Cell Sci *121*, 2783-2793.

Fish, J.L., Kosodo, Y., Enard, W., Paabo, S., and Huttner, W.B. (2006). Aspm specifically maintains symmetric proliferative divisions of neuroepithelial cells. Proc Natl Acad Sci U S A *103*, 10438-10443.

Fong, K.W., Choi, Y.K., Rattner, J.B., and Qi, R.Z. (2008). CDK5RAP2 Is a Pericentriolar Protein That Functions in Centrosomal Attachment of the {gamma}-Tubulin Ring Complex. Mol Biol Cell *19*, 115-125.

Graser, S., Stierhof, Y.D., and Nigg, E.A. (2007). Cep68 and Cep215 (Cdk5rap2) are required for centrosome cohesion. J Cell Sci *120*, 4321-4331.

Griffith, E., Walker, S., Martin, C.A., Vagnarelli, P., Stiff, T., Vernay, B., Al Sanna, N., Saggar, A., Hamel, B., Earnshaw, W.C.*, et al.* (2008). Mutations in pericentrin cause Seckel syndrome with defective ATR-dependent DNA damage signaling. Nat Genet *40*, 232-236.

Hayflick, L., and Moorhead, P.S. (1961). The serial cultivation of human diploid cell strains. Exp Cell Res *25*, 585-621.

Ishikawa, H., Kubo, A., and Tsukita, S. (2005). Odf2-deficient mother centrioles lack distal/subdistal appendages and the ability to generate primary cilia. Nat Cell Biol *7*, 517-524.

Jackson, A.P., Eastwood, H., Bell, S.M., Adu, J., Toomes, C., Carr, I.M., Roberts, E., Hampshire, D.J., Crow, Y.J., Mighell, A.J.*, et al.* (2002). Identification of microcephalin, a protein implicated in determining the size of the human brain. Am J Hum Genet *71*, 136-142.

Jackson, A.P., McHale, D.P., Campbell, D.A., Jafri, H., Rashid, Y., Mannan, J., Karbani, G., Corry, P., Levene, M.I., Mueller, R.F.*, et al.* (1998). Primary autosomal recessive microcephaly (MCPH1) maps to chromosome 8p22-pter. Am J Hum Genet *63*, 541-546.

Kemp, C.A., Kopish, K.R., Zipperlen, P., Ahringer, J., and O'Connell, K.F. (2004). Centrosome maturation and duplication in C. elegans require the coiled-coil protein SPD-2. Dev Cell *6*, 511-523.

Khodjakov, A., Rieder, C.L., Sluder, G., Cassels, G., Sibon, O., and Wang, C.L. (2002). De novo formation of centrosomes in vertebrate cells arrested during S phase. J Cell Biol *158*, 1171-1181.

Kirkham, M., Muller-Reichert, T., Oegema, K., Grill, S., and Hyman, A.A. (2003). SAS-4 is a C. elegans centriolar protein that controls centrosome size. Cell *112*, 575-587.

Kumar, A., Girimaji, S.C., Duvvari, M.R., and Blanton, S.H. (2009). Mutations in STIL, encoding a pericentriolar and centrosomal protein, cause primary microcephaly. Am J Hum Genet *84*, 286-290.

Kwon, M., Godinho, S.A., Chandhok, N.S., Ganem, N.J., Azioune, A., Thery, M., and Pellman, D. (2008). Mechanisms to suppress multipolar divisions in cancer cells with extra centrosomes. Genes Dev *22*, 2189-2203.

La Terra, S., English, C.N., Hergert, P., McEwen, B.F., Sluder, G., and Khodjakov, A. (2005). The de novo centriole assembly pathway in HeLa cells: cell cycle progression and centriole assembly/maturation. J Cell Biol *168*, 713-722.

Lange, B.M., and Gull, K. (1995). A molecular marker for centriole maturation in the mammalian cell cycle. J Cell Biol *130*, 919-927.

Leidel, S., Delattre, M., Cerutti, L., Baumer, K., and Gonczy, P. (2005). SAS-6 defines a protein family required for centrosome duplication in C. elegans and in human cells. Nat Cell Biol *7*, 115-125.

Leidel, S., and Gonczy, P. (2003). SAS-4 is essential for centrosome duplication in C elegans and is recruited to daughter centrioles once per cell cycle. Dev Cell *4*, 431-439.

Li, H.S., Wang, D., Shen, Q., Schonemann, M.D., Gorski, J.A., Jones, K.R., Temple, S., Jan, L.Y., and Jan, Y.N. (2003). Inactivation of Numb and Numblike in embryonic dorsal forebrain impairs neurogenesis and disrupts cortical morphogenesis. Neuron *40*, 1105-1118.

Li, K., and Kaufman, T.C. (1996). The homeotic target gene centrosomin encodes an essential centrosomal component. Cell *85*, 585-596.

Luders, J., and Stearns, T. (2007). Microtubule-organizing centres: a re-evaluation. Nat Rev Mol Cell Biol *8*, 161-167.

Mahoney, N.M., Goshima, G., Douglass, A.D., and Vale, R.D. (2006). Making microtubules and mitotic spindles in cells without functional centrosomes. Curr Biol *16*, 564-569.

Marshall, W.F., Vucica, Y., and Rosenbaum, J.L. (2001). Kinetics and regulation of de novo centriole assembly. Implications for the mechanism of centriole duplication. Curr Biol *11*, 308-317.

Mayor, T., Stierhof, Y.D., Tanaka, K., Fry, A.M., and Nigg, E.A. (2000). The centrosomal protein C-Nap1 is required for cell cycle-regulated centrosome cohesion. J Cell Biol *151*, 837-846.

Megraw, T.L., Kao, L.R., and Kaufman, T.C. (2001). Zygotic development without functional mitotic centrosomes. Curr Biol *11*, 116-120.

Mocali, A., Giovannelli, L., Dolara, P., and Paoletti, F. (2005). The comet assay approach to senescent human diploid fibroblasts identifies different phenotypes and clarifies relationships among nuclear size, DNA content, and DNA damage. J Gerontol A Biol Sci Med Sci *60*, 695-701.

Nakagawa, Y., Yamane, Y., Okanoue, T., and Tsukita, S. (2001). Outer dense fiber 2 is a widespread centrosome scaffold component preferentially associated with mother centrioles: its identification from isolated centrosomes. Mol Biol Cell *12*, 1687-1697.

Nakajima, D., Saito, K., Yamakawa, H., Kikuno, R.F., Nakayama, M., Ohara, R., Okazaki, N., Koga, H., Nagase, T., and Ohara, O. (2005). Preparation of a set of expression-ready clones of mammalian long cDNAs encoding large proteins by the ORF trap cloning method. DNA Res *12*, 257-267.

Nigg, E.A. (2006). Cell biology: a licence for duplication. Nature *442*, 874-875.

Nigg, E.A. (2007). Centrosome duplication: of rules and licenses. Trends Cell Biol *17*, 215-221.

Northcutt, R.G., and Kaas, J.H. (1995). The emergence and evolution of mammalian neocortex. Trends Neurosci *18*, 373-379.

O'Connell, K.F., Caron, C., Kopish, K.R., Hurd, D.D., Kemphues, K.J., Li, Y., and White, J.G. (2001). The C. elegans zyg-1 gene encodes a regulator of centrosome duplication with distinct maternal and paternal roles in the embryo. Cell *105*, 547-558.

Paintrand, M., Moudjou, M., Delacroix, H., and Bornens, M. (1992). Centrosome organization and centriole architecture: their sensitivity to divalent cations. J Struct Biol *108*, 107-128.

Palazzo, R.E., Vogel, J.M., Schnackenberg, B.J., Hull, D.R., and Wu, X. (2000). Centrosome maturation. Curr Top Dev Biol *49*, 449-470.

Pelletier, L., O'Toole, E., Schwager, A., Hyman, A.A., and Muller-Reichert, T. (2006). Centriole assembly in Caenorhabditis elegans. Nature *444*, 619-623.

Pelletier, L., Ozlu, N., Hannak, E., Cowan, C., Habermann, B., Ruer, M., Muller-Reichert, T., and Hyman, A.A. (2004). The Caenorhabditis elegans centrosomal protein SPD-2 is required for both pericentriolar material recruitment and centriole duplication. Curr Biol *14*, 863-873.

Pfaff, K.L., Straub, C.T., Chiang, K., Bear, D.M., Zhou, Y., and Zon, L.I. (2007). The zebra fish cassiopeia mutant reveals that SIL is required for mitotic spindle organization. Mol Cell Biol *27*, 5887-5897.

Pihan, G., and Doxsey, S.J. (2003). Mutations and aneuploidy: co-conspirators in cancer? Cancer Cell *4*, 89-94.

Potter, M. (2008). Brief historical sketch of chromosomal translocations and tumors. J Natl Cancer Inst Monogr, 2-7.

Quintyne, N.J., Reing, J.E., Hoffelder, D.R., Gollin, S.M., and Saunders, W.S. (2005). Spindle multipolarity is prevented by centrosomal clustering. Science *307*, 127-129.

Rakic, P. (1995). A small step for the cell, a giant leap for mankind: a hypothesis of neocortical expansion during evolution. Trends Neurosci *18*, 383-388.

Rauch, A., Thiel, C.T., Schindler, D., Wick, U., Crow, Y.J., Ekici, A.B., van Essen, A.J., Goecke, T.O., Al-Gazali, L., Chrzanowska, K.H.*, et al.* (2008). Mutations in the pericentrin (PCNT) gene cause primordial dwarfism. Science *319*, 816-819.

Reilova-Velez, J., and Seiler, M.W. (1984). Abnormal cilia in a breast carcinoma. An ultrastructural study. Arch Pathol Lab Med *108*, 795-797.

Sawin, K.E., Lourenco, P.C., and Snaith, H.A. (2004). Microtubule nucleation at non-spindle pole body microtubule-organizing centers requires fission yeast centrosomin-related protein mod20p. Curr Biol *14*, 763-775.

Serrano, M., Lin, A.W., McCurrach, M.E., Beach, D., and Lowe, S.W. (1997). Oncogenic ras provokes premature cell senescence associated with accumulation of p53 and p16INK4a. Cell *88*, 593-602.

Singla, V., and Reiter, J.F. (2006). The primary cilium as the cell's antenna: signaling at a sensory organelle. Science *313*, 629-633.

Sluder, G., Thompson, E.A., Miller, F.J., Hayes, J., and Rieder, C.L. (1997). The checkpoint control for anaphase onset does not monitor excess numbers of spindle poles or bipolar spindle symmetry. J Cell Sci *110 ( Pt 4)*, 421-429.

Strnad, P., and Gonczy, P. (2008). Mechanisms of procentriole formation. Trends Cell Biol *18*, 389-396.

Stryke, D., Kawamoto, M., Huang, C.C., Johns, S.J., King, L.A., Harper, C.A., Meng, E.C., Lee, R.E., Yee, A., L'Italien, L.*, et al.* (2003). BayGenomics: a resource of insertional mutations in mouse embryonic stem cells. Nucleic Acids Res *31*, 278-281.

Tang, B.L. (2006). Molecular genetic determinants of human brain size. Biochem Biophys Res Commun *345*, 911-916.

Tornoczky, T., Semjen, D., Shimada, H., and Ambros, I.M. (2007). Pathology of peripheral neuroblastic tumors: significance of prominent nucleoli in undifferentiated/poorly differentiated neuroblastoma. Pathol Oncol Res *13*, 269-275.

Trimborn, M., Bell, S.M., Felix, C., Rashid, Y., Jafri, H., Griffiths, P.D., Neumann, L.M., Krebs, A., Reis, A., Sperling, K.*, et al.* (2004). Mutations in microcephalin cause aberrant regulation of chromosome condensation. Am J Hum Genet *75*, 261-266.

Tsou, M.F., and Stearns, T. (2006a). Controlling centrosome number: licenses and blocks. Curr Opin Cell Biol *18*, 74-78.

Tsou, M.F., and Stearns, T. (2006b). Mechanism limiting centrosome duplication to once per cell cycle. Nature *442*, 947-951.

Uetake, Y., Loncarek, J., Nordberg, J.J., English, C.N., La Terra, S., Khodjakov, A., and Sluder, G. (2007). Cell cycle progression and de novo centriole assembly after centrosomal removal in untransformed human cells. J Cell Biol *176*, 173-182.

van Haaften-Day, C., Russell, P., Davies, S., and Brammah-Carr, S. (1992). An in vitro study of ovarian atypical proliferating (borderline) serous tumors. Int J Gynecol Cancer *2*, 41-48.

Venkatram, S., Tasto, J.J., Feoktistova, A., Jennings, J.L., Link, A.J., and Gould, K.L. (2004). Identification and characterization of two novel proteins affecting fission yeast gamma-tubulin complex function. Mol Biol Cell *15*, 2287-2301.

Verde, I., Pahlke, G., Salanova, M., Zhang, G., Wang, S., Coletti, D., Onuffer, J., Jin, S.L., and Conti, M. (2001). Myomegalin is a novel protein of the golgi/centrosome that interacts with a cyclic nucleotide phosphodiesterase. J Biol Chem *276*, 11189-11198.

Vladar, E.K., and Stearns, T. (2007). Molecular characterization of centriole assembly in ciliated epithelial cells. J Cell Biol *178*, 31-42.

Vorobjev, I.A., and Chentsov Yu, S. (1982). Centrioles in the cell cycle. I. Epithelial cells. J Cell Biol *93*, 938-949.

Woods, C.G., Bond, J., and Enard, W. (2005). Autosomal recessive primary microcephaly (MCPH): a review of clinical, molecular, and evolutionary findings. Am J Hum Genet *76*, 717-728.

Yang, J., Adamian, M., and Li, T. (2006). Rootletin interacts with C-Nap1 and may function as a physical linker between the pair of centrioles/basal bodies in cells. Mol Biol Cell *17*, 1033-1040.

Yang, Z., Loncarek, J., Khodjakov, A., and Rieder, C.L. (2008). Extra centrosomes and/or chromosomes prolong mitosis in human cells. Nat Cell Biol *10*, 748-751.

Zhong, X., Liu, L., Zhao, A., Pfeifer, G.P., and Xu, X. (2005). The abnormal spindle-like, microcephaly-associated (ASPM) gene encodes a centrosomal protein. Cell Cycle *4*, 1227-1229.

Zhong, X., Pfeifer, G.P., and Xu, X. (2006). Microcephalin encodes a centrosomal protein. Cell Cycle *5*, 457-458.

Zimmerman, S., and Chang, F. (2005). Effects of {gamma}-tubulin complex proteins on microtubule nucleation and catastrophe in fission yeast. Mol Biol Cell *16*, 2719-2733.